Guilherme Mendes Ferreira

Bachelor of Science in Micro and Nanotechnologies Engineering

"Eco-energy Smart Card": A human-interactive all paper based, mechanical energy harvester

Dissertation submitted in partial fulfillment of the requirements for the degree of
Masters in Micro and Nanotechnologies Engineering

Adviser: Dr. Suman Nandy, Research Investigator, CENIMAT – i3N

Co-Adviser: Prof. Luís Miguel Nunes Pereira, Associate Professor, DCM, FCT-UNL

Examination comittee:

Chairperson: Prof. Rodrigo Ferrão de Paiva Martins, Full Professor, DCM, FCT-UNL

Raporteur: Prof. Pedro Miguel Cândido Barquinha, Assistant Professor, DCM, FCT-UNL

Member: Dr. Suman Nandy, Research Investigator, CENIMAT – i3N

FACULDADE DE CIÊNCIAS E TECNOLOGIA
UNIVERSIDADE NOVA DE LISBOA

October 2019

“Eco-energy Smart Card”: A human-interactive all paper based, mechanical energy harvester

Acknowledgments

As I prepare to clear yet another career milestone, this Master Thesis requires me to acknowledge all the people who made these years replete with memories. Through hard work and self-realization “The sky is limit” as I continue towards my professional career. Even though we can only go as far as we aspire, no one can achieve success alone. In my university career this couldn’t be more true.

Firstly, and I would not forgive myself if this section started any differently, special thanks to my family. Thanks to my father and my mother for raising me and being effectively responsible for what I have become. You are also the best support anyone could have ever asked for. Also, to my brother, for being my best friend and the funniest person I know. My life would be very sad and boring if you were not here. To my grandmother, Margarida, with whom I have lived these past five years. Thanks for helping me in my day-to-day life. Your youthfulness at such an age is contagious and I wish I could be like you as I grow older. To my cousins, Inês, Bruno and Diogo who are like brothers (and sister) to me and whom I care a lot. Then, to my both my godparents Florinda and Filipe, my grandparents Manuel, Irene, to Marito, Dolores, Carolina and Francisco, you are just as responsible for making me a happy person as anyone can be. Also, to my grandfather Joaquim, who has Alzheimer’s disease but whom I know would be extremely proud of this moment.

Secondly, I would like to thank Professor Elvira Fortunato and Professor Rodrigo Martins, for the promotion of portuguese nanotechnology around the world and for the creation of this course that I am about to graduate from. You have given a path to a man who did not know what he wanted to do with his life.

Thirdly, to the wonderful people, I have met during these five years in college. Especially to my closest friends: Guilherme Castelo, Luís Bettencourt, Renato Nora, Joan Concha, Mafalda Pina, Inês Tavares, João Vieira, Joana Rodrigues e Mariana Moniz. Without you, nothing would have been the same. Thanks for all the good times, for all the parties and all the support we gave each other for studying and other college projects.

To Preeta Ananthanarayanan, Cesar Oliveira and João Vieira (once again!) for making my Erasmus trip, the greatest experience I have ever had.

Moreover, thanks to Suman Nandy and Sumita Goswami for being the most pleasant surprise during these five years. You are one of the kindest and hardworking people I know. Thanks for all the close support you have given me. Thanks for ALWAYS being available. Thanks for exposing me to the scientific world, by assisting me with my first conference experience and publishing exposure. Thanks for all the knowledge both in science and in life. I truly am thankful, and I want to make you proud.

I would also like to thank professor Luís Pereira, for giving me the opportunity to work in a project which I loved contributing to.

And finally, thanks to the long (very long!) list of people both in CENIMAT and CEMOP who never refused to help and always did it with a smile on their faces. It truly was a pleasure working with you!

Abstract

Nowadays, it is imperative that modern society finds sustainable ways to harvest energy. This means society is forced to look to new ways to generate and store energy, while reducing, simultaneously, the stress on raw materials demand and the amount of waste generated. Our research tackles these two points by making close to zero e-waste clean energy harvesting devices. The core idea behind it is based on the mechano-responsive charge-transfer mechanism and energy-transfer process in π-conjugated polymer at the organic-metal interface layer. A localized forced deformation of the interface has been applied against the polymer surface, allowing charge transfer between material interfaces. The experimental results demonstrated that during contacting force, the conjugated polymer film shows electrical output through the charge transfer mechanism within metal/polymer interfaces. Flexible and low-cost energy harvesting devices built have an active layer constituted by a PANi/cellulose composite which was tapped together to a charge collector layer, that was made from a paper based metallic electrode. These devices have a total maximum power density and maximum current density of 1.75 Wm^{-2} and 33.5 mA m^{-2}, respectively. Towards the practical applicability, these devices are able to light up to 40 blue LEDs as well as a commercial humidity sensor.

Keywords: Paper Electronics, Clean Energy, Mecahno-stimulli, Charge Transfer, Zero e-waste, Polyaniline/Cellulose system.

Resumo

Nos dias que correm, é imperativo que a sociedade encontre alternativas sustentáveis para gerar energia. Isto significa que seremos forçados a encontrar novas formas de produção de energia e ao mesmo tempo reduzir a procura por novas matérias primas e a quantidade de lixo gerado. A nossa investigação combate esses dois problemas através do desenvolvimento de dispositivos com baixo impacto ao nível do lixo eletrónico. O princípio por detrás do funcionamento destes dispositivos é baseado na resposta a um estímulo mecânico que gera um mecanismo de transferência de carga entre polímeros π-conjugados quando em contacto com um metal. Uma pressão localizada aplicada sobre a superfície do polímero, resulta numa transferência de carga entre o polímero e o metal. Dispositivos de geração de energia low-cost e flexíveis foram construídos através da junção de uma camada ativa, composta pelo compósito PANi/celulose e uma camada coletora de carga que compreende elétrodos que possuem papel como substrato, sendo posteriormente também encapsulado com papel. Estes dispositivos demonstraram uma densidade de potência máxima de 1.75 W m^{-2} e densidade de corrente máxima no valor de 33.5 mA m^{-2}. Com vista a uma abordagem mais prática, com um destes dispositivos foi possível ligar simultaneamente 40 LEDs azuis e também um sensor comercial de humidade.

Palavras-chave: Eletrónica de Papel, Energia Limpa, Transferência de Carga Mecanicamente Estimulada, Baixo Resíduo Eletrónico, Sistema Polianilina/Celulose

Contents

List of Figures

List of Tables

List of Abbreviations

AC – Alternating Current

AFM – Atomic Force Microscopy

AL – Active Layer

AN – Aniline

APS – Ammonium Persulfate

B – Benzenoid

CSA – Camphor–10–Sulfonic Acid

CCL – Charge Collector Layer

CPD – Contact Potential Difference

e-waste – Electronic Waste

EDS – Energy Dispersive Spectroscopy

EFM – Electrostatic Force Microscopy

FESEM – Field Emission Scanning Electron Microscopy

FCP – Functionalized Chromatography Paper

HOMO – Highest Occupied Molecular Orbital

KPFM – Kelvin Probe Force Microscopy

LUMO – Lowest Unoccupied Molecular Orbital

PANi – Polyaniline

Q – Quinoid

SEM – Scanning Electron Microscopy

TENG – Triboelectric Nanogenerator

U.S. – United States

WCP – Whatman Chromatography Paper

List of Symbols

I – Current

e – Elementary charge

I_{max} – Maximum current density

P_{max} – Maximum power density

V_{oc} – Open circuit voltage

P – Power

Φ_{probe} – Probe potential

R – Resistance

Φ_{sample} – Sample potential

I_{sc} – Short circuit current

$\Delta\Phi$ – Work function difference

Φ – Work function

$\Delta\delta$ Height of the cantilever from the surface

$\Delta\varphi$ - Phase shift

C – Capacitance

Z – Impedance

Motivation and Objectives

The biggest challenge of the XXI century is the urge to fight climate change by revolutionizing our carbon-based energy system while concurrently reducing the amount of waste products and the continuous dependence on raw materials. The urgency of the matter was recognized at an International Level when in 2015 all the state members of the United Nations signed the "2030 Agenda for Sustainable Development". Therefore, there must be a worldwide effort to tackle these issues. (**Figure M.1**)

Figure M.1 – Sustainable development goals defined by the United Nations for the "2030 Agenda for Sustainable Development".

Technological advances from here on must have in mind these prerogatives (sustainable goals) while promoting economic growth and general well-being of an increasing population both in numbers and in resource demand, namely in the field of green energy applications. With the treat of climate change, society is forced to face head on the energetic crisis and make the change to green, with zero e-waste, energy technologies. For that new concepts must be explored, as well as technical approaches and materials.

One of those materials is paper, that has been widely studied in recent years in the field of paper electronics especially because of its availability, simple fabrication, recycling properties, low-cost and lightweight. Although several applications of paper in electronics are being developed, such as supercapacitors, microfluidic devices, smart sensors, even energy harvesting purposes, there is still a gap when it comes to applying paper to mechanical harvesting energy systems.

Therefore, the specific goal of this master research proposal is to develop a mechano-responsive energy harvester based on a paper platform, that is low-cost, flexible and whose waste is easily treatable and recyclable, bringing it closer to the "zero-e waste" challenge. In this specific case, paper was functionalized with polyaniline (PANi), which is a conjugated, conductive polymer. Together with cellulose as a composite system, the polymer has very good conductive properties and energy harvesting potential. The final product will then be tested in order to study the input-output relationship of the energy transduction process.

This work is one contribution to fight climate change (goal #13) and the waste management issues while at the same time advancing surely in making our way to get access to clean and accessible portable energy (goal #7), technological innovation at industrial level (goal #9), that can potentially generate new markets in the energy sector (goal #8), and sustainable cities and communities (goal #11).

1. Introduction

The World is currently being challenged with the toxic legacy of disposable electronic gadgets from a tech-hungry society. The high production allied with the short lifespans of these technologies results in towering electronic waste (e-waste) which is becoming an enormous threat to our planet. The apprehension regarding e-waste comes from the fact that it involves a high cost and complex treatment to deal with it in an environmentally manner, due to its hazardous and polluting demeanor.[1-3] According to the U.N. in 2016 the world produced a combined amount of 44.7 million metric tons of e-waste and this number is expected to rise to 52.2 million tons in 2021.[4] The biggest producers of e-waste are mainly OCDE countries than end up sending their waste to least developed or under developed countries. (**Figure 1.1**)

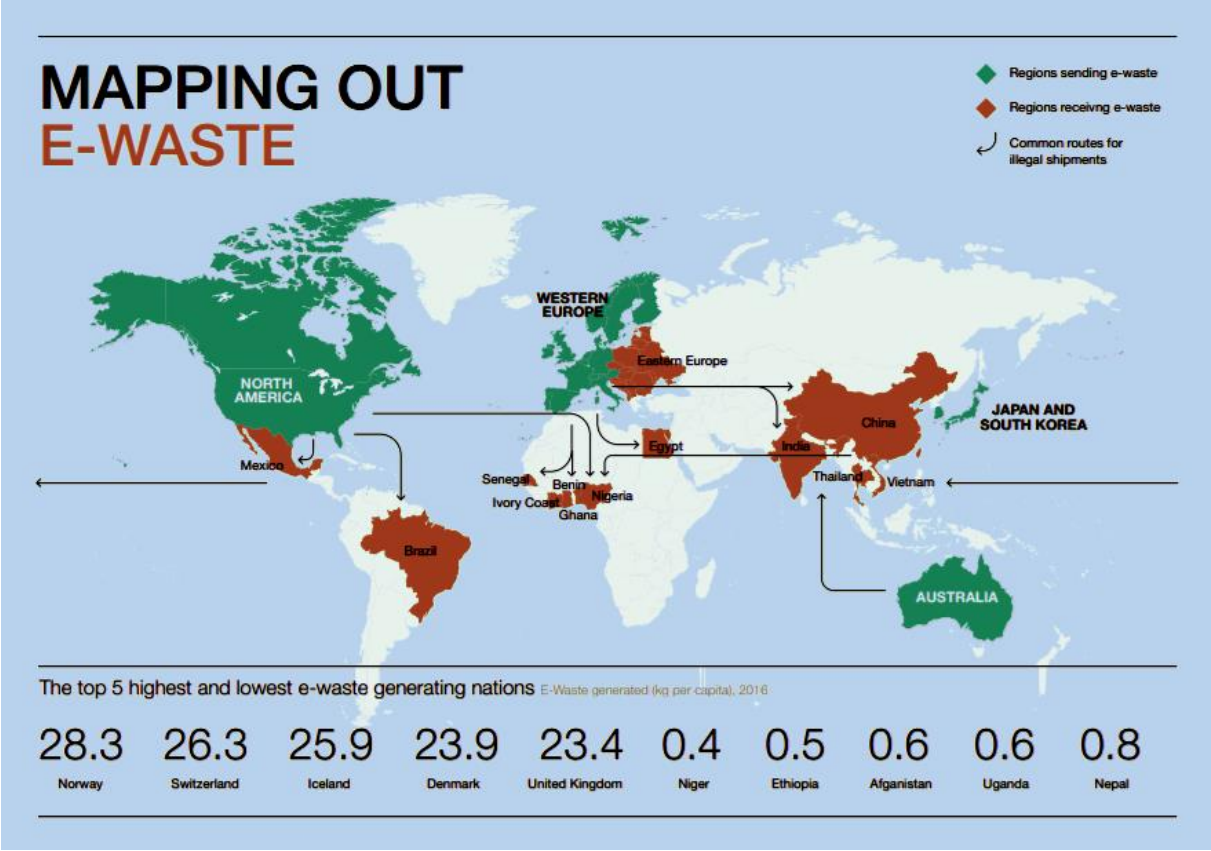

Figure 1.1 – Worldwide e-waste flow and quantity of e-waste produced per inhabitant in 2016[5]

It is of paramount importance that mankind advances towards green and sustainable technologies, cutting down e-waste, and concurrently not neglecting the fast upgrading of the digitalization state-of the art. Having this in mind, scrutinizing new strategies to deal with climate change and the energetic crisis can be facilitated if the scientific community employs the "zero e-waste" paradigm and envisions technologies which are environmentally flawless and economically viable.

1.1 Paper's role in Circular Economy and Upcoming Technologies.

The demand for raw materials has increased with the world's growing population. However, the supply of raw materials is limited and being used at full scale. In addition, extracting and using excess amount of raw materials, which cannot be recycled, has a major impact on the environment. Waste products are a big consequence of the continuous raw supply search. The European Union alone produces more than 2.5 billion tons of waste each year, from which only 36% is recycled.[6]

To counteract that the concept of circular economy was created. Circular economy is a system of production and consumption aimed at maximizing sharing, reusing, repairing and recycling materials, making the best possible use of the product.

Waste prevention and re-use of materials and products could save the European Union industry up to 600 billion euros, create as many as 858 000 jobs, while reducing total greenhouse gas emissions by 2-4%.[7] Shifting towards a more circular economy, would reduce the stress on the environment, while boosting economic growth. (**Figure 1.2.1 a)**). The consumer's quality of life would also be improved with the introduction of more durable and innovative products. A circular economy relies on a "Reduce, Reuse and Recycle" system, which is very much appreciated by the pulp and paper industry. (**Figure 1.2.1 b)**).In this aspect paper is a widely commercial material which is very much part of our daily lives, used in essential commodities. The material has revealed itself as a promising substrate material for new electronica purposes, because of its availability, which results in lower-cost, simple fabrication and recycling properties. Recent studies using paper electronics include its use in various areas such as: flexible supercapacitors,[8, 9] paper transistors,[10, 11] and microfluidic analytical devices[12].

Indeed, paper is a trending material in the field of flexible electronics, some papers have recently been released comprising the use of paper as a substrate for energy harvesting applications. Most of these works used paper as functionalized substrate with conductive active material: carbon nanotubes, graphene and even conducting polymers,[13-15] revealing that indeed paper can act as a network for charge carriers.

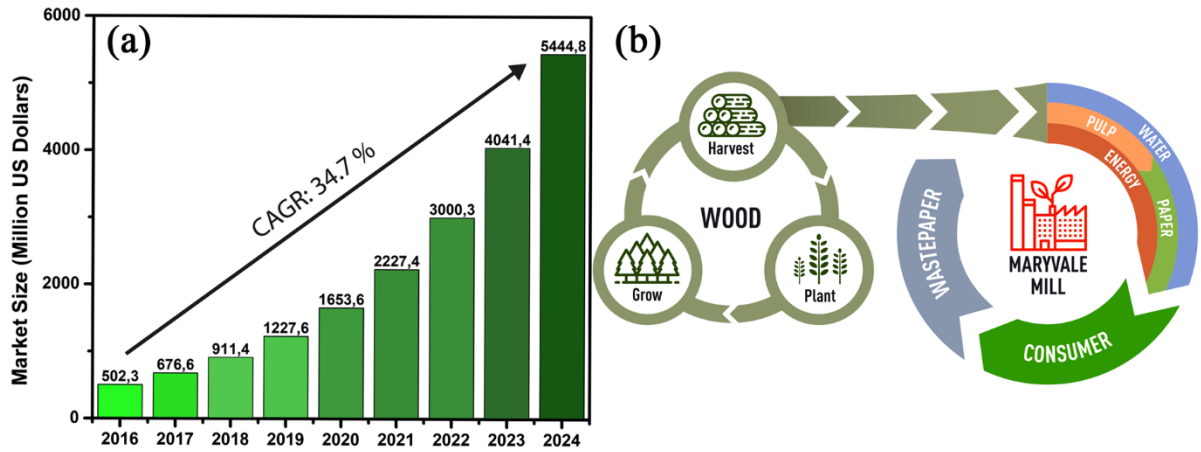

Figure 1.1.1 – **(a)** Paper Electronics market size growth and correspondent forecast until 2024 (values in million US dollars).[16] **(b)** Circular economy approach to paper manufacturing [17]

At the same time the popularity of flexible electronics including wearables and human interactive technologies has been thriving as a trending topic, being a very fertile field for the growth of new ideas for flexible energy harvesting purposes. There is therefore a huge potential for the development of new mechanical energy harvesting strategies, using flexible human interactive technologies.

1.2 Conjugated Polymers

Conjugated polymers are organic macromolecules with delocalized π-electrons arising from overlapping of p-orbitals, which have brought about a lot of attention in numerous smart electronics applications namely, display devices like PLED's (polymer light-emitting diodes),[18,19] supercapacitors,[20] electrochromic windows,[21] field-effect transistors (OFET's), [22, 23] sensors,[24, 25] data storage,[26, 27] etc. For energy harvesting purposes, conjugated polymers like Polypyrrole and Polyaniline have already been employed. They have both been used for supercapacitors, pseudo capacitors, rechargeable batteries and piezoelectric systems. In all of these, the polymers were used as electrode materials, due its high conductivity and flexibility. [28, 29] Nevertheless they have also been used as an active layer. [30]

They have revealed themselves as a good candidate for organic electronics because of their ability to control the physical, electrical and chemical properties trough doping-dedoping processes in their molecular design. In addition, a central issue in their electrical properties is the delocalized π-electron bonds which can create a good charge transfer mechanism between the network.[31] Among these conjugated polymers, polyaniline (PANi) is one of the more investigated materials because of its elementary synthesis, high environmental stability and low-cost system.[32]PANi has also shown great results when it comes to the enhancement of electrical properties when in composite structure with other substrates opening doors to the fabrication of good electroactive hybrids.[29]

Therefore it would be of great interest to combine both the conjugated polymers and paper into a single active material to act as a mechano-responsive energy harvester and as a consequence launch a new type of green technology whose residue would be easily treated making our way to technologies which have close to zero e-waste. Polyaniline is already reported to improve the conductivity of paper by several units of magnitude.[29]

1.3 Charge Transfer Mechanism

The core-idea behind the energy harvesting system using a PANi/cellulose composite is to explore the mechano-responsive charge transfer mechanism of π-conjugated polymers at the metal/polymer interface. A localized pressure at the metal/polymer surface is applied which will result in a rise of localized electron density causing Fermi-level pinning and, consequently, charge carriers will transmute from polymer to the nearest available energy state, which is the metallic electrode. When pressure is released the polymer networks will expand which will result in a localized electron scaricity. The neighbouring regions, where the electron density is much higher, will balance out this scarcity by hopping mechanism, enabling for a new pressure cycle to begin.

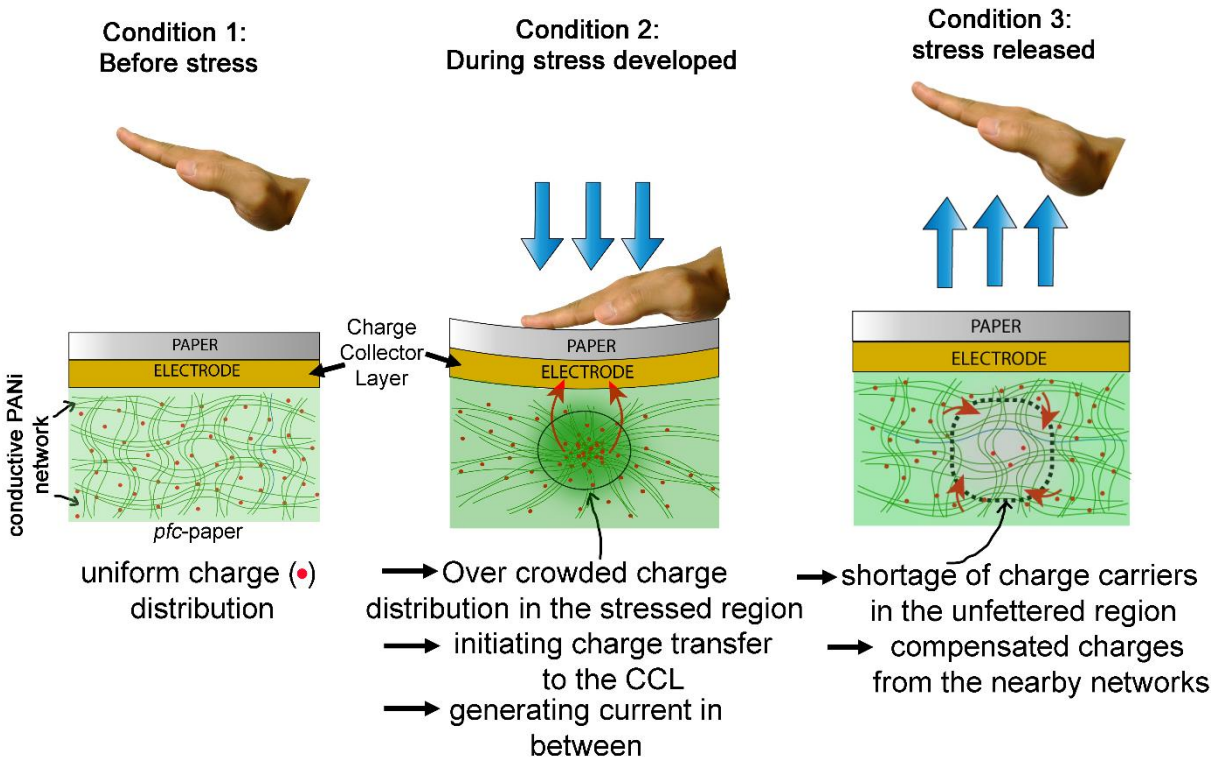

Figure 1.3.1 – Schematic illustration of charge transfer mechanism stages: **(a)** before stress, no charge transfer mechanism taking place; **(b)** during stress-induced condition; electrons jump to the electrode due to high electron density caused by a localized pressure; **(c)** stress release condition; after the pressure is released the polymer tries to recover its original form, resulting in a localized electron scarcity that will be compensated by electrons from neighboring polymer region.

In the present work, an elementary, low-cost paper-based energy harvester, responsive to human touch-interaction is presented, targeting to harness the wasted mechanical energy dissipated by our body motion into an electrical output signal. Functionalization of chromatography paper via *in-situ* polymerization process using the drop-cast technique at room temperature was applied. The PANi/cellulose composite was tapped together to a metallic electrode (paper-based), the former working as an Active Layer (AL) and the later as a Charge Collector Layer (CCL). The (paper-based) prototypes were made in the form of an "eco-energy smart card", applicable for human touch-interactive energy harvester. Our prototype device can glow up to 40 LED's and charge up capacitors whose energy was then used to power a commercial humidity sensor.

1.4 Mechanical Energy Harvesting

Society's concern in developing sources of green energy has grown widely in the last few decades.[33, 34] In conjunction with the more conventional forms of renewable energy like solar, wind, geothermal, nuclear, etc, mechanical energy, is beginning to reveal itself as an interesting form of energy harvesting. Researcher's appetite towards this form of energy is due to its big presence in our daily lives, since it can be harvested from, human motion,[35] wind,[36] rain,[37] etc.

Piezoelectric and triboelectric materials endure as trending designing tools for energy generation applications. These materials harvest mechanical energy by generation of an electric output, through contact electrification and electrostatic induction, as a response to a mechanical stimulus.[10] Contact electrification is a phenomenon based on the height of the energy levels of materials and can be described as a process in which charge transfer is achieved when two different materials are brought into contact and then separated repeatedly.[38]

Piezoelectricity is an effect that is verified in materials that develop an electric field as a response to a mechanical stress or strain. At rest the structure's electrostatic centers (positive and negative) are positioned in such a way that they cancel each other out, resulting in an electrically neutral molecule. Before subjecting the material to an external stress, the centers of the negative and positive charges of each molecule coincide – resulting into an electrically neutral molecule. When pressure is applied, the whole structure gets deformed, resulting in a displacement of the electrostatic centers generating little dipoles. In these materials the reverse effect is also verified, meaning, the emergence of a stress or strain as result of an applied electric field.[39,40]

The triboelectric effect is in part caused by a contact adhesion, when two materials are brought into each other. There is a charge, can be both ions and electrons, transfer in order to compensate the electrochemical potential. There are plenty of factors that can influence the triboelectric process, making it difficult to get a definite physical description of the phenomenon. Nevertheless, there are plenty of applications that involve the triboelectric effect. The charge transfer mechanism is more closely related to the triboelectric effect. Moreover, it is not a piezoelectric system because the charge transfer mechanism defined above is related to the increase of a localized charge density instead of the polarity of inter charges[41-43]

Piezoelectric generators have previously been studied and used in a broad array of applications, namely: in pacemakers,[44,45] for tire pressure monitoring systems, [46,47] in the concept of smart houses,[48, 49] etc. In the field of energy harvesting applications, they have been associated to wearable technology, like shoes or cloths that use the dissipated work from muscles to generate power, [50-51] but also are known to harvest energy from environmental sources like rain [53] and wind.[54]

In the field of energy harvesting, triboelectric nanogenerators are starting to trend, especially because these can be light weighted, flexible and portable resulting in a huge variety of studies. These devices have been reported to have successfully harvested energy from wind,[55] water waves,[56] human body motion, [57, 58] even studied in order to trying to adapt these to Mars environment and possibly used in a future space mission.[59]

The triboelectric nanogenerators (TENG's) are trending in the field of energy harvesting. There have already been some triboelectric energy harvesting systems based on paper, Yang, *et al* (2015) [60] and

Yao, *et al*, (2016) [61] have both reported such systems with power density of 140 mW m^{-2}. There are four kinds of TENG's: vertical contact mode, lateral sliding contact, single electrode and free-standing triboelectric layer mode. In the single electrode TENG, only one of the electrodes is associated to the active layer, while the other one can be considered the ground. Wu, *et al* (2019)[62] and Cui, *et al (2018)* [63] have developed single electrode TENG with power density of 4.97 mW m^{-2} and 22.5 mW m^{-2}.

The electrical performance of both piezoelectric energy harvesters and triboelectric energy harvesters is characterized by a high output voltage yet small current making these more suitable for small powered circuits. This can limit the use of this technology for higher scale power supply applications. This problem may be solved by integrating in the system the supercapacitor technology, which can be adapted to be light weighted, flexible and portable.[64]

2. Materials and Methods

The whole process for the fabrication of the "eco-energy smart card" involved three phases: paper functionalization, electron manufacturing and device assembly. A schematic resuming all the processes involved in the fabrication of the "eco-energy smart card" is shown in the Annexes section. (**Figure A.1.1)**

2.1 Main Reagents

Aniline monomer (AN; 99,5%, Sigma-Aldrich), ammonium persulfate (APS; 99.99%, Sigma-Aldrich), camphorsulfonic acid (CSA; 98%, Sigma-Aldrich) and hydrochloric acid (HCl; ~37%, Alfa Aesar) are the main reagents used in the synthesis of polyaniline (PANi). All the reagents were used as received without any further purification. Throughout all the experiments and washing procedures only deionized (DI) water (obtained from Millipore Elix Advantage 3 purification system) was used.

2.2 Pixelating the Paper

The drop-casting technique, in this kind of paper, allows for an uncontrolled spread of solution throughout the paper. To address this issue square-shaped wells (12.5 x 12.5 mm^2) were wax-printed in an array form (e.g. 7 x 4) by using solid wax (Ref:108R00935, Black) in a normal office printer (Xerox ColorQube 8580) in order to contain the solution to a precisely known area (10x10 mm^2). After printing the paper was heated at 100 °C so that the wax would diffuse and form a barrier to contain the drop-casted solutions. A snapshot of the wax printed pattern on the paper is shown in the schematic of the process in the Annexes section. (**Figure A.1.1**)

2.3 Functionalization of paper with polyaniline

For the functionalization several types of paper were tried out, including: Whatman™, Chromatography Paper (WCP), Grade: 1 CHR; CavalinhoTM, Drawing Paper; MAB, "Papel Manteigueiro"; Office Paper, NOTEIT and Aquarelle-Acrilique Paper, CANSON.

Each pixelized area printed on the paper was individually used for *in-situ* functionalization. The polymerization was done by a two-step drop-casting method. The mechanism is a simple one. The first step is to prepare two precursor solutions. One solution is an oxidizing aqueous solution (Solution A) made from the addition of 0.9128g of APS to 10ml of DI water. Afterwards 100 µL of HCl was added to the solution, which was then put under mechanical agitation for 10 minutes to make a homogenous mixture. Afterwards a surfactant solution was prepared (solution B). It started by adding 0.4646g of CSA to 20 ml of DI water. Then 365 µl of AN was added to the mixture, which was then left to steer also for 10 minutes. The functionalization was done according to the process used by Goswami, *et al*, 2019. [30]

The WCP was only functionalized on one side. The solutions were drop-casted on top of the paper in a Solution A:Solution B ration of 1:2. The amount of solution A being 12 µL and the amount of solution B being 24 µL, for each paper pixel. The reaction took place at room temperature and only needed 5 minutes to be completed. After this time, the color of the paper can visually be seen, changing to a dark green color, which is indicative of the emeraldine salt of PANi. Once the functionalization process was over the samples were washed with DI water and methanol, they were then left to dry at room temperature.

2.4 Fabrication of Electrodes

In the meantime, it was also necessary to make flexible electrodes so that the active layer of PANi-cellulose could be integrated in the concept of eco-energy card. Several types of electrodes were used (carbon, copper, silver, gold and aluminum). This was done in order to study the influence of different electrode types. The purpose was to check which interface was better suited for energy harvesting purposes. The silver (CRSN2442 AG INK,Coated Screen Inks) and carbon (CRSN2664 C INK, Sun Chemical) electrodes were screen-printed on paper (Whatman™, Chromatography Paper, Grade: 1CHR) and later dried on a hot plate at 100 °C (for 15 and 40 minutes for silver and carbon respectively). The aluminum electrode used was obtained from a package of Tetrapak™, the copper electrode was

made from applying copper tape on the surface of paper. Finally, for the gold electrode, the e-beam evaporation technique was used. In this process, it was first deposited a layer of Titanium, because its adhesion to paper is better than the gold. Both depositions were made under a vacuum level as high as 2×10^{-6} mbar. For the Ti deposition a current of 0.05A and a rate of 0.06 nm/sec was used which resulted in a final thickness of 10nm. For the Au deposition a current of 0.09A and a rate of 0.12 nm/sec was used which resulted in a final thickness of 70 nm, resulting in a total electrode thickness of 80nm. A snapshot of all the paper-based types of electrodes used is shown in the Annexes section. (**Figure A.1.2**)

2.5 Fabrication of "Eco-energy Smart-Card"

For the fabrication of device, different layers were integrated into one. The PANi functionalized paper, which constituted the active layer (AL), was made into contact with the Charge Collector Layer (CCL), that consisted in the paper-based electrode. The polyaniline functionalized paper was in direct contact with the metallic electrode. The third and fourth layers make the encapsulation of the device, the encapsulation used was from paper, in order to simulate an actual smart card. All the layers were tapped together with commercial office tape. The cards differed between themselves in the type of electrode used (material) and the area of the functionalized paper (1x2, 2x2 and 3x2 pixelized configurations were used). In **Figure 2.5.1** a schematic of al the layers of the "eco-energy smart card" is presented.

Figure 2.5.1 – Schematic of the devices built, comprehending three layers: the active layer (AL) that has the FCP, the charge collector layer (CCL) which consists of the paper based electrodes and the encapsulation layer, which is also paper-based.

2.6 Characterization Techniques

Morphological and compositional analyses were conducted using a field emission scanning electron microscope (FESEM-FIB, Carl Zeiss Auriga Crossbeam microscope) with energy dispersive x-ray spectroscopy (EDS, Oxford XMax 150). The chemical structures of the samples were also characterized by Raman spectroscopy (Renishaw Qontor InVia Raman microscope) using the 532 nm excitation laser line with 10% of the maximum laser power (50 mW) and 1s exposure time for each 10 accumulations. Atomic force microscopy (AFM) measurements were performed within an Asylum Research MFP-3D Stand-alone using commercial Pt-Ir tip coated probes. All the data was recorded under different applied bias, implying throughout calibration of the probe beforehand. The data was analyzed offline with the Asylum Research tools, developed within the IGOR Pro 6.22A data analysis software. The mechano-electrical studies were performed by recurring to a standard oscilloscope, (Tektronix TBS 2022). For the measurement of the force magnitude applied to the card a circuit associated to a programmed Arduino board (Arduino Uno Rev3 (ATMega 328P)) and a force sensor (Interlink Electronics, FSR 406) was put into place.

3. Results and Discussion

As it was mentioned in **section 2.3**, the functionalization process is quite simple and fast. It is our prerogative to functionalize the paper substrate with polyaniline. Its formation has origin in the combination between several reduced and oxidized blocks of aniline monomer. It is possible to regulate through controlled synthesis parameters the amount of oxidized and reduced monomers in the polymer, which determines the different phases of polyaniline. There are three different phases: leucoemeraldine, (the fully oxidized polyaniline state), it is non-conductive and colorless; pernigraniline (the fully reduced polyaniline state), it is a dark blue/violet insulating polymer, and emeraldine, which has equal quantity of reduced and oxidized monomer.

For our purposes, it is important to have polyaniline in doped emeraldine form (the conductivity can be tuned with doping de-doping processes) due to its semi-conducting properties. The synthesis of polyaniline can be performed by several techniques: Oxidative Chemical Synthesis, Interfacial Polymerization, Microemulsion Polymerization, Solid-state synthesis, electrochemical polymerization and enzymatic synthesis.[65] In this case it was decided to go for the Oxidative Chemical Synthesis because it is fast, simple and the polyaniline can be functionalized into a huge variety of substrates. The reaction is described as follows:

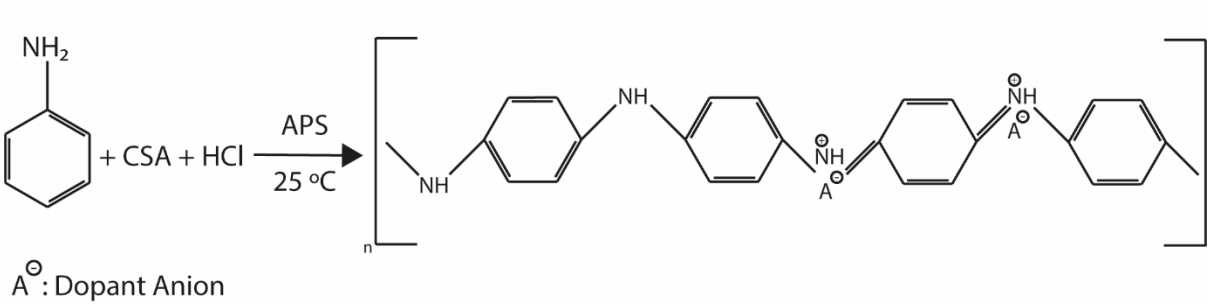

Figure 3.1 – Schematic of the reaction: *in-situ* polymerization of aniline through redox reaction and its protonation.

3.1 Chemical and Morphological Analyses

In **Figure 3.1.1(a)** a schematic of the functionalization procedure is showed, whereas in **Figure 3.1.1(b)** shows the Functionalized Chromatography Paper (FCP) on both sides. The dark green color indicates that the polymerization occurred not only at the surface but also inwardly, due to capillarity effects. Both reactants penetrate the cellulose microstructure allowing the polymerization reaction to occur everywhere. As mentioned in the experimental section, several types of paper were functionalized. The WCP (Whatman Chromatography Paper) allowed for better emeraldine functionalization results, because it is pure cellulose, with no additives, which allowed for no interference of extra reactants in the polymerization. Furthermore, in the WCP the existing hydrogen bonds of the basic cellulose unit make the cellulose/PANi bounding more compact and well-formed. Other papers were tried but the dark green colour, characteristic from the emeraldine phase of PANi was not verified. The porosity of this kind of raw paper permitted functionalization on both sides, since the solutions get diffused through the paper's structure, giving full functionalization to it.

In the reaction described above APS acts has a redox reaction initiator.[66] There are several types of oxidants that can be used, among these: potassium dichromate, hydrogen peroxide, cerium sulfate and ferric chloride.[67] The reason why APS is preferred is because it has a higher oxidation potential (E0=1.94V), whereas the others, have an oxidation potential of 1.23, 1.78, 1.72 and 0.77V respectively.[65]

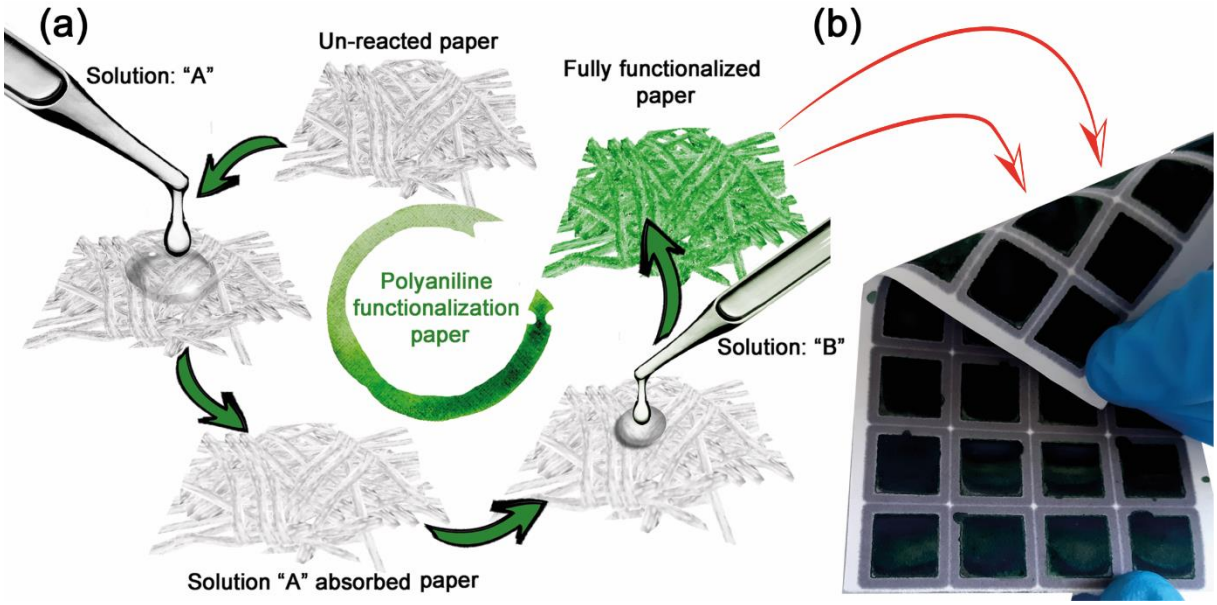

Figure 3.1.1 – (a) Schematic representing all the WCP functionalization steps; **(b)** Functionalized Chromatography Paper (FCP) shown on both sides

The monomers are a neutral entity, and when the reduction and oxidizing processes happen there is a delocalization of two electrons which allows for the formation of benzenoid rings linked together by the amine groups (-NH-), and quinoid rings bonded together by the imine moieties (-N=).[68] These functional groups which are present all over the polymer chain, allow for an easier doping with both metallic cations and protons (p-type and n-type). Each oxidation state can exist in the form of its base or its salt by protonation with an organic or inorganic acid. It is well known that protonation of emeraldine base with aqueous HCl, results in an increase in conductivity by several orders of magnitude .[69] What happens is that the HCl will interact with the imine groups (which will lose one of the electrons from the nitrogen lone pair), leading to the formation of polycations which will influence the creation of a polaron conduction band. In opposition to other conducting polymers the cation will be mostly associated to the nitrogen.[70] In this case it was also decided to use CSA as an additive, this anionic surfactant will influence the polymerization to occur around a micelle and thus determining the final morphology of the conducting polymer. It also has an influence in the stability of the polymer, by adding a hydrophobic component it is expected less influence of moisture, which is important because the less moisture, the less subsequent hydrolysis and therefore less deprotonation. CSA will also act as a de-doping agent, which differs from HCl, which is a primary doping, from the fact that it influences the polymer in a way that the number of electrons presented in the polymer backbone persist unaltered. These alterations can be advantageous or not, depending on the primary dopant and secondary dopant combination preformed. Nonetheless using it as de-doping agent can greatly increase the conductivity of Polyaniline.[71]

In order to observe the formation of PANi/cellulose composites throughout the paper, FESEM imagining was realized on both sides of the paper, as shown in **Figure 3.1.2**. It is possible to observe that, although the bottom surface looks like a smoother coating, it is still functionalized with similar microstructures to those from the front side. There has been an aggregation of several particles leading to PANi granules. One of the most frequent configurations of PANi is indeed the granular morphology with a "globular structure".[72] This paper surface can be compared with a raw WCP SEM image in the Annexes section from the schematic englobing all the fabrication processes (**Figure A.2.1**).

Their geometric shape is a direct consequence of the reaction's parameters like molar ratios between monomer and oxidizing agent.[73] The CSA has a hydrophilic head, which is composed by the "–SO_3H", and a hydrophobic tail, which is part of the rest of the molecule, that gives it an amphiphilic configuration. In this way the molecules can act both as a surfactant and as an organic dopant.[74] The aggregation of micelles, as a discontinuous phase, is a direct consequence of the dispersion of dopant in

water. When adding aniline monomer these tend to form a complex surrounding the micelles. There is also the influence of the induction period, which corresponds to the time needed for accumulation and self-organization of nucleates (aniline oligomer). Shorter periods of induction usually result in chaotic agglomeration of nucleates, while longer periods favor assembly of microstructures in columns forming one-dimensional structures. Shorter periods of induction are associated with the use of strong oxidants, and high monomer concentration in acidic medium (ph<2.5 and c > 0.1 mol L^{-1}). Organization becomes extremely difficult because the phenazine does not have time to organize before the polymer chains start to form.[73] Longer periods of induction are usually obtained by using weaker oxidants.[75]

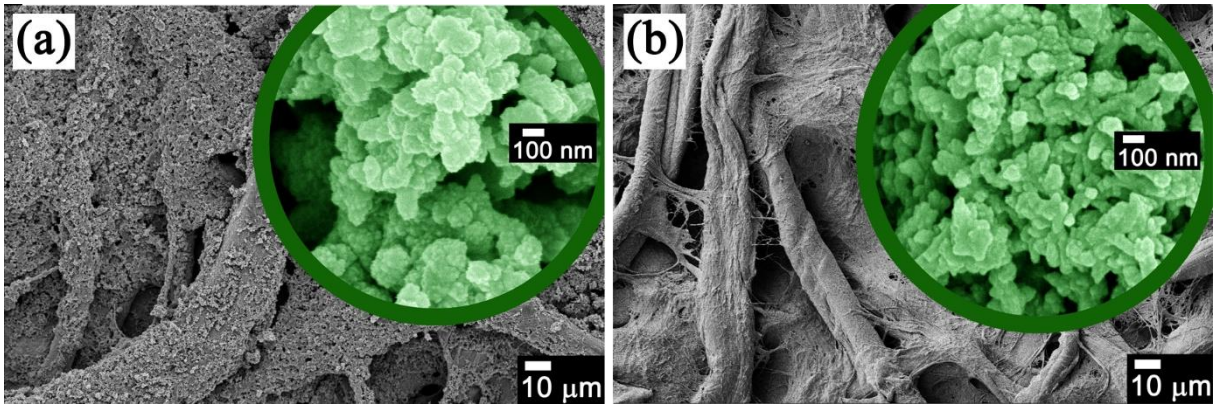

Figure 3.1.2 – (a) FESEM images of the FCP, from the front (drop-cast side); **(b)** FESEM image from the back of the FCP

The reaction time does not affect greatly the morphology of the microstructures. The results obtained by Zhang and Wan (2002) [76], using similar conditions (the only difference is being the presence of HCl during the reaction) for *in-situ* reactions, demonstrate that similar weight ratio of CSA and Aniline result in nanotubes, with micelle growth by elongation. Moreover, for a CSA/Aniline ration of 2:1, the structures obtained were similar to those obtained in this thesis. Thus, it is possible to infer, that the presence of HCl (as a strong acid) in the reaction is the main cause for the tendency of agglomeration verified. From other studies, it was seen that applying weak acids represses the formation of nanoparticles yielding one dimensional configuration instead. [77] A possible explanation for the chaotic organization is that the addition of HCl to the oxidizing solution will provide a Cl^- anions which will increase the ionic strength of the medium and has a consequence decrease the regular organization of nucleates, as shown by previous studies. [78, 79]

In association to SEM imaging an EDS elemental mapping on FCP (**Figure 3.1.3**) was also performed. In the mapping mainly carbon and oxygen is seen, which can be associated to the quinoid and benzenoid rings (carbon) of the emeraldine salt and to the cellulosic structure of the substrate (oxygen and carbon). The presence of Sulphur and chlorine results from doping agents utilized in the polymer synthesis, which came from CSA and HCl, respectively. This corroborates the idea that a cellulose-PANi composite was indeed formed.

Raman Spectroscopy (**Figure 3.1.4)** was also performed to make chemical analyses to the functionalized paper (on both sides) and to raw chromatography paper (control sample). It is possible to observe that the spectra is similar on both sides of the functionalized paper. The position of the peaks typically reveals the identity of doped conductive PANi, as summarized below [80, 81]: The strong band at 1591 cm^{-1} is due to the C═C stretching vibrations in the Quinoid (Q) rings. The shoulder peak at 1562 cm^{-1} can be attributed to C─C stretching in quinoid units whereas the strong peak at 1478 cm^{-1} is representing the C═N stretching vibration in Q rings. The band at 1336 cm^{-1} with a shoulder at 1371 cm^{-1} is associated with the presence of C~N+● vibrations in the delocalized polaronic structures. The weak peak at 1246 cm^{-1} is ascribed to the C─N stretching vibrations of Benzenoid (B) rings. The very strong intensity band at 1164 cm^{-1} is due to the C─H bending vibrations of the semi-quinoid rings which corresponds to the cation-radical segments. The peaks at 878 and 810 cm^{-1} arise from C─N─C wagging and or B ring deformations in the polarons or bipolarons of emeraldine salt structure of the polymeric backbone and

substituted B ring deformations respectively. The bands at 609 and 575 cm^{-1} are attributed to the vibrations of B ring deformations and phenoxazine-type units respectively. Comparing with the WCP control sample spectrum it is possible to confirm the differences and that paper composites were produced through in-situ polymerization.

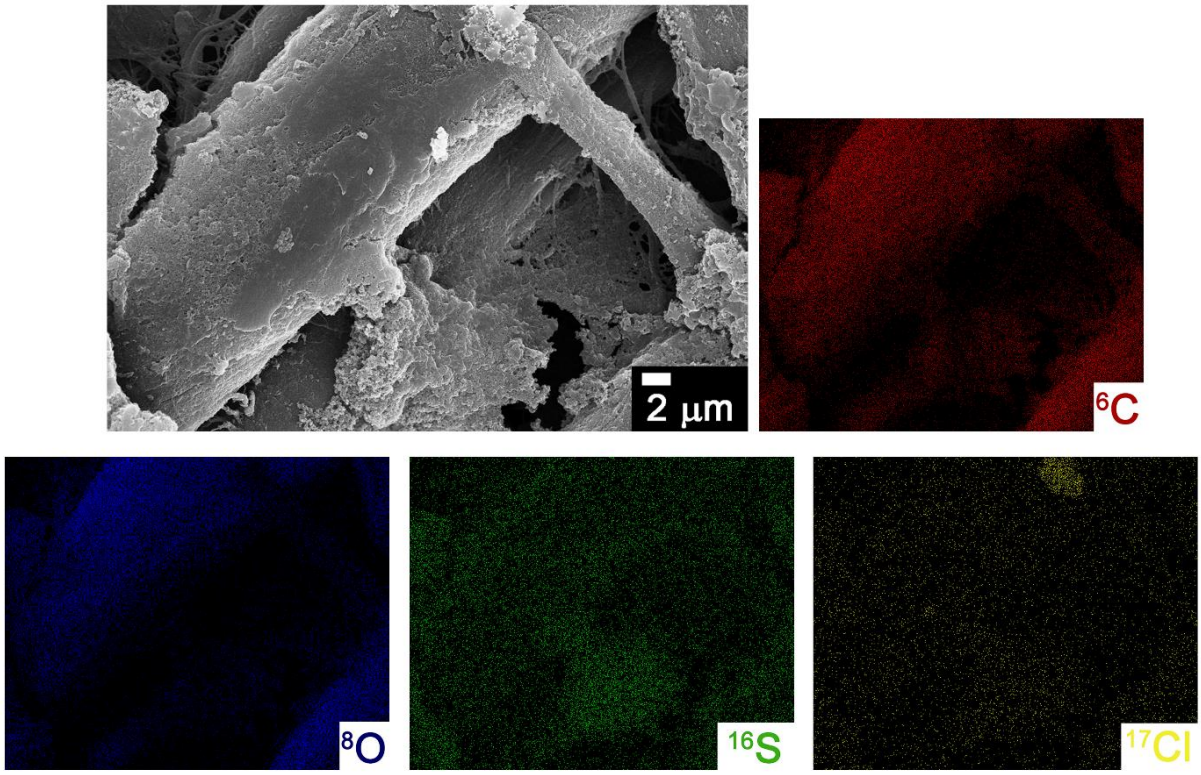

Figure 3.1.3 – EDS elemental mapping of the FCP

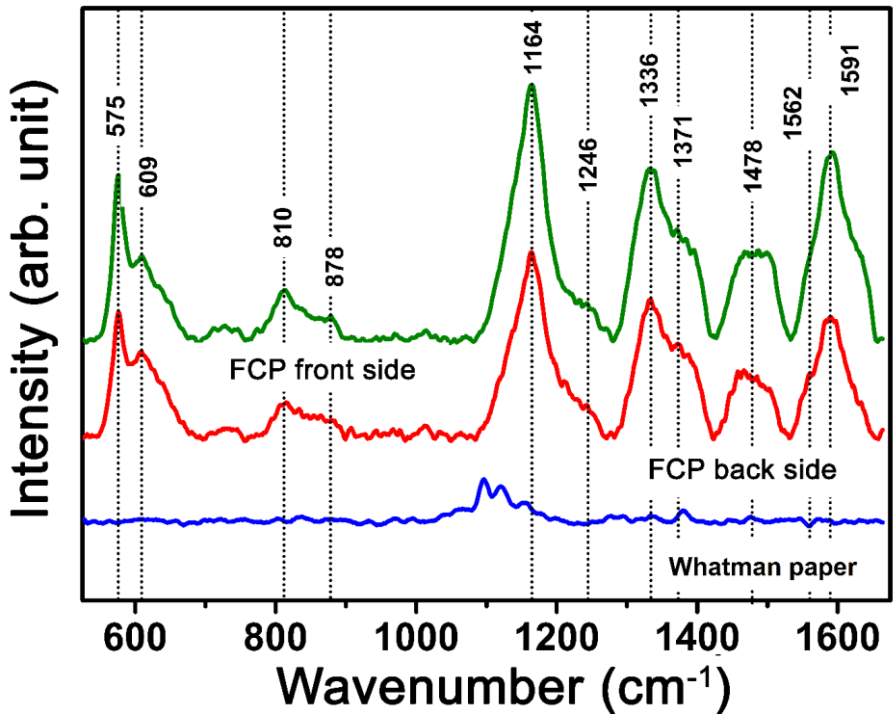

Figure 3.1.4 – Results obtained through Raman Spectroscopy performed on the front side and the back side of FCP as well in a raw WCP.

3.2 Electrical Analyses

Interestingly, after the functionalization of WCP through *in-situ* polyaniline polymerization, the FCP shows very good conductivity of 0.1 S m^{-1}. The cross-section and lateral resistances of the functionalized paper were both measured with values around 370 and 590 Ω, respectively, as shown in **Figure 3.2.1**. As previously mentioned, the conductivity of a sample depended strongly on the level of protonation from doping processes. These gave rise to the appearance of polaronic structure in the monomer molecules which overlap with the polarons of its neighbors influencing the movement of π electrons through the backbone of the polymer.

Figure 3.2.1 – **(a), (b)** Lateral and cross-sectional resistance of the FCP, respectively

Electrostatic Force Microscopy (EFM) analyses were done in order to visualize the localized charge distribution images of the FCP, compared to the raw WCP. The EFM is a technique commonly employed in electrical surface analyses to obtain data concerning the surface potential or the charge distribution. The main feature of the EFM is a cantilever that is responsive to long-distance electrostatic force discrepancies. This technique takes up a dual-pass measurement approach. A first pass is done in order to scan the topography properties of the surface, by scanning it in tapping mode. In the second pass the cantilever scans the surface following the path of first pass but keeping a certain distance (Δδ height, in this case 50 nm), from the sample (parallel line) through an external applied bias on the tip (5V). In the first pass the deflection in the cantilever works under van der Waals force, whereas in the second pass these deflections are caused by the change of phase and oscillation when it scans over static charges. As a result, the resonance frequency of the cantilever will change influenced by the electrostatic forces between the tip and the sample. The oscillation of the cantilever will result in phase changes in the laser signal that will be detected by the photodetector. The photodetector will then generate an electrical signal which will be processed to generate a final mapping. Charge trapping in the embedded systems is explicatory from the color mapping in EFM images, where color scale is defined by phase difference, Δφ (in degree) = contact potential difference between AFM probe and sample surface. [82]

$$\Delta\varphi \propto {}^{1}\Big/_{\frac{\partial^2 C}{\partial Z^2}} \quad (1)$$

Where, C and Z are probe-sample capacitance and separation respectively. **Figure 3.2.2 (a)** and **Figure 3.2.2 (b)** shows the topography images for FCP and WCP, and corresponding charge distribution image is shown in **Figure 3.2.2 (c)** and **Figure 3.2.2 (d),** respectively. Corresponding histogram of EFM images has been shown in **Figure 3.2.2 (e)**. From the histogram it can be observed that there is a lot more phase shifting from the functionalized paper (**Figure 3.2.2 (d)**), in comparison to the raw sample (**Figure 3.2.2 (c)**) which indicates the presence of a different electrostatic surface after the *in-situ* functionalization of the WCP, corroborating that a PANi/cellulose composite was indeed formed. The cantilever deflection is most likely associated to the polaron created by the cation presented in the amine

group. Also, a widening feature of histogram of FCP depicts uniform distribution of embedded trapped charge due to *in-situ* functionalization of paper. (**Figure 3.2.2 (e)**).

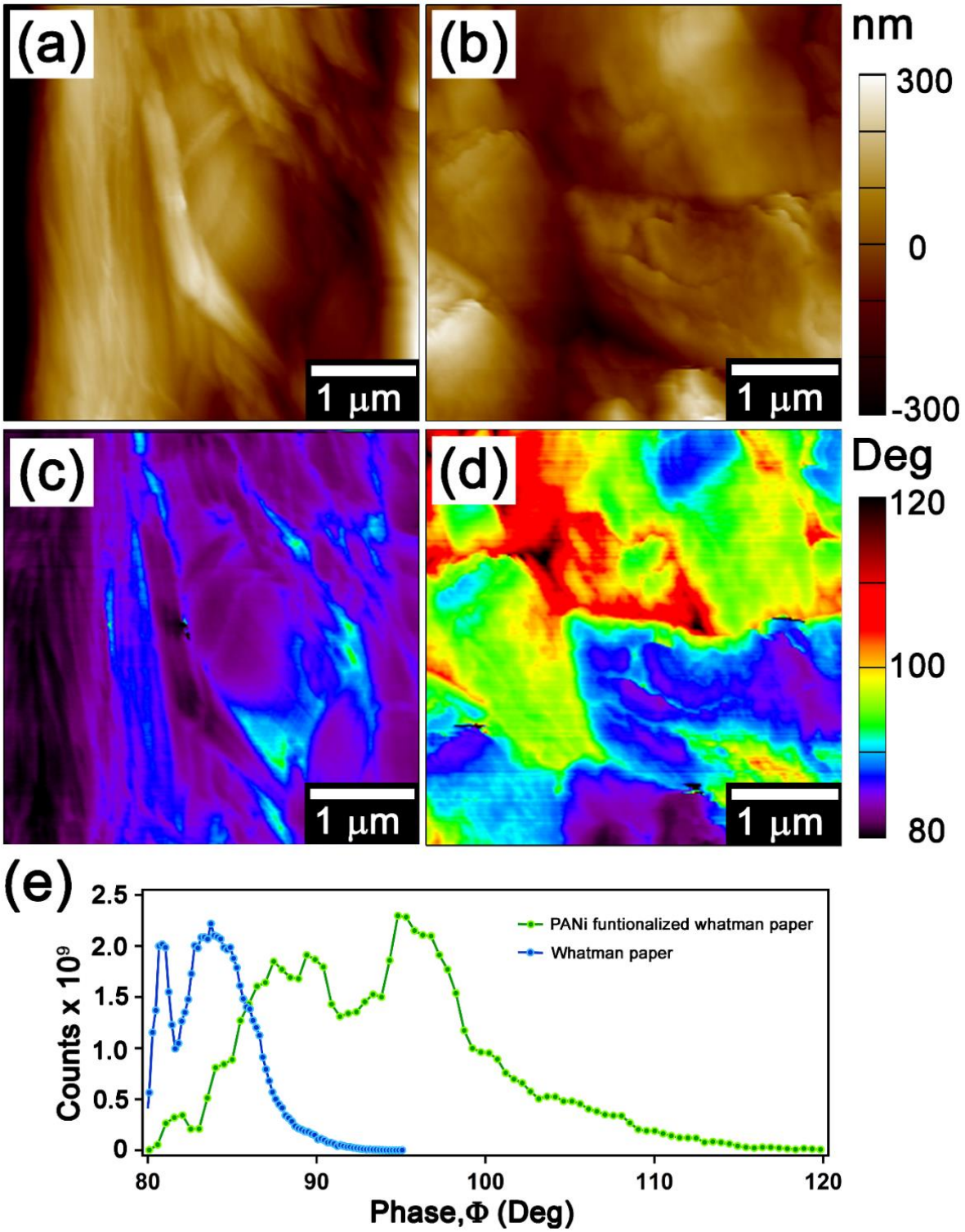

Figure 3.2.2 – **(a), (b)** Show the topography images of raw WCP and FCP, respectively; **(c), (d)** Localized trapped charge distribution map of raw WCP and FCP, simultaneously measured in EFM mode. Phase difference in analytical image with color indicating the difference of trapped charge distribution compared with raw WCP and FCP. **(e)** Corresponding histogram of EFM map.

3.3 “Eco-Energy Smart Card” Performance

The “eco-energy smart cards” were designed in a way, that will allow electrical energy to be generated under mechanical stimuli through charge transfer mechanism in the PANi/cellulose networks. Taking into account the “zero e-waste” challenge, the energy harvesting devices (**Figure 3.3.1**) were built in a low-cost and clean process. As mentioned earlier, the FCP was placed into direct contact to the several types of electrodes (aluminum, carbon, copper, gold and silver) and then both were encapsulated, which is necessary in order to protect both the Active Layer (AL) and the Charge Collector Layer (CCL). The protective encapsulation layers were made from either hard paper or tracing paper. Copper tape or carbon fiber has been used to make a contact between CCL and the measuring device connector to facilitate output electric performance. In some cases, more than one contact was made in each card because the copper tape is not the most resistant material and it could get damaged form the tapping while measuring the output voltage under mechanical stimulus.

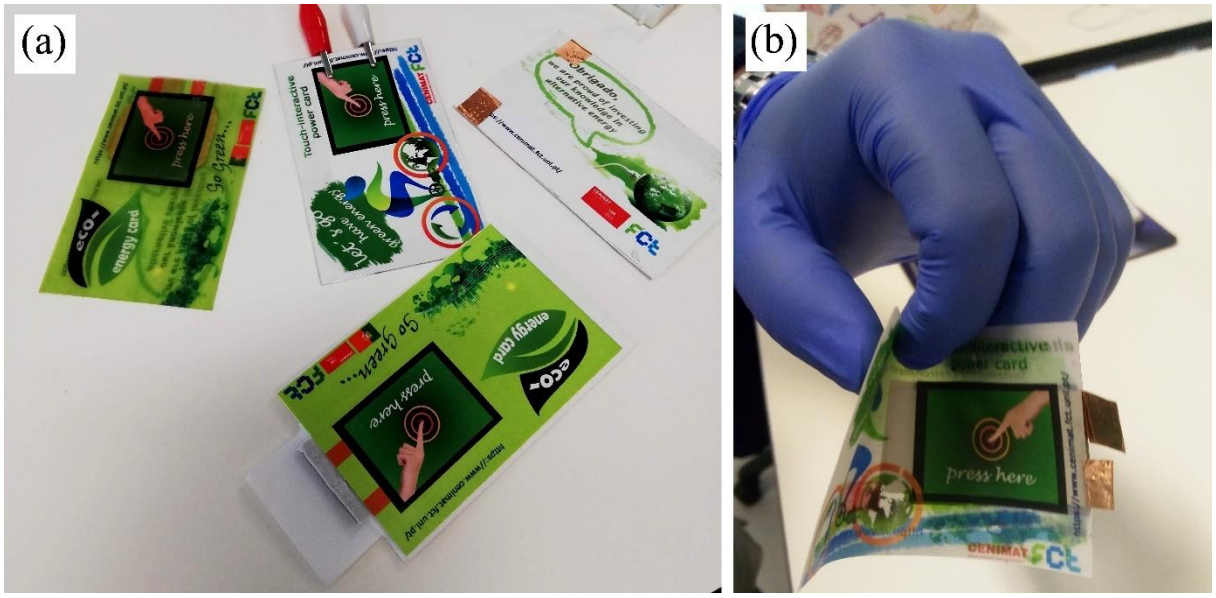

Figure 3.3.1 – **(a)** The devices were built in paper-basis concept which allowed them to have a cheap manufacturing, recycling properties and be **(b)** flexible

When a force is applied on top of the functionalized paper surface, there is a deformation in the molecular structure leading to a physical approximation of the polymer chains. The localized chain deformation increases locally the concertation of charge carriers that will create the Fermi level (highest energy-level in the valence band that can be occupied by electrons at 0° K) pinning which will further initiate a charge transfer mechanism from the highly crowded PANi/cellulose area to the nearest more stable system (metallic electrodes).[83] When stress is released there is a decrease in charge density at the surface which will result in unpinning of the Fermi level and consequently stop the charge transfer. This is because of the expansion of polymer chains which will result in a localized electronic scarcity. This electronic scarcity is then balanced by charge diffusion through the polymer backbone from neighboring chains which have higher electronic density. Therefore, it is possible to infer that the charge transfer mechanism is mainly dependent on four factors: effective area onto which the force is applied, magnitude of applied force, frequency, and metallic material used on the CCL.

Therefore, the performance of the “eco-energy smart card” is highly dependent on these factors. In the following it is presented a meticulous study of all these factors and how they individually affect the performance of the device.

I. Output performance depending on the effective area

The AL area influence on the device's output performance is very intuitive. Higher effective area will result in larger regions initiating a charge transfer mechanism at metal/polymer interface layer, causing larger amount of charge carriers translocating from the polymer to the electrode, hence generating more current. One of the ways to improve the effective area of applied force is also to use devices with a larger active layer. **Figure 3.3.2** clearly shows, that the open-circuit output voltage (V_{oc}) increases linearly with the total area of the AL. Pixelating the paper was useful in this particular study, for an easier quantification of the effective area. For a device with an area of 2 × 1 pixels, the voltage was approximately 25-30 V, 2 × 2 presented a value close to 50-60 V and 70-75 V for a 2 × 3 matrix, each pixel as a total functionalized area of 1 cm^2. The same type of electrode (Cu electrode) was used in all these measurements. Both the frequency and the applied force were maintained constant in the different measurements made. A device with WCP as an AL, coupled with two electrodes, has been tested for mechano-responsive electrical output. The measured electrical output was near few millivolts which is comparatively very low with respect with our device. (See in Annexes section, **Figure A.4.1**).

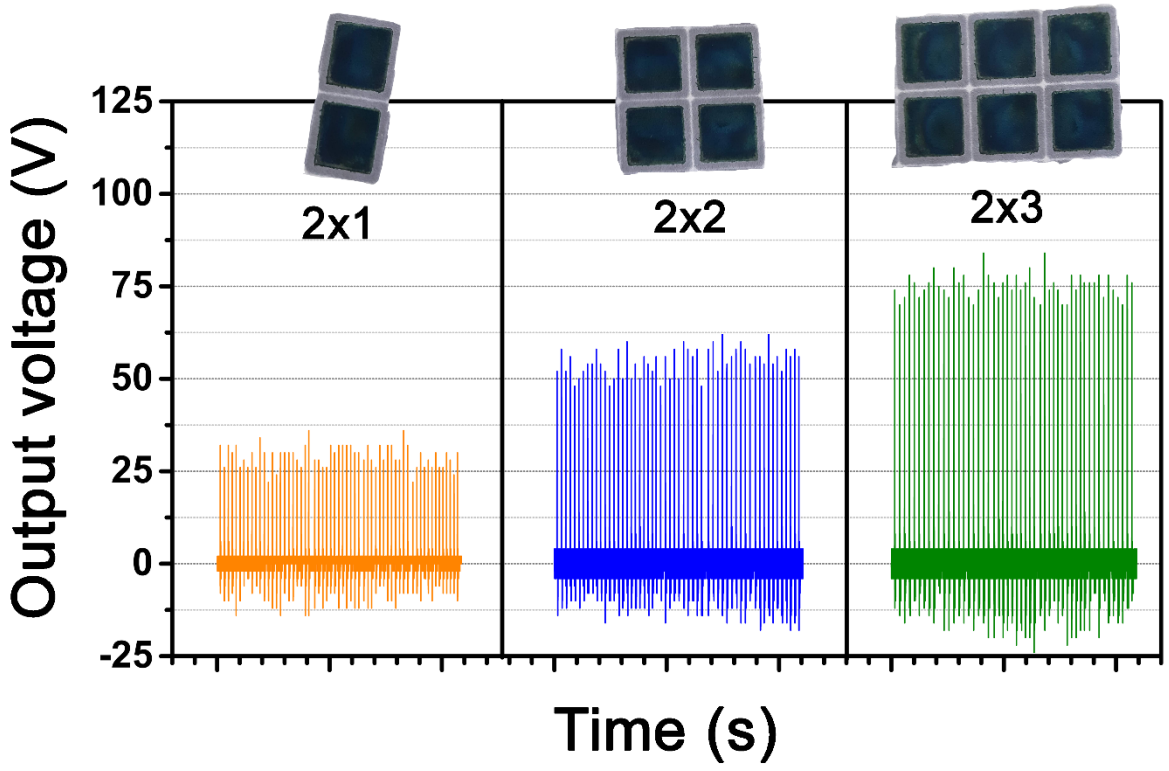

Figure 3.3.2 - Electrical output (V_{oc}) recorded upon periodic mechanical stimuli. The V_{oc} was recorded for different pixelated matrices of FCP as an AL, under the same applied force, which is shown above. It can be observed that V_{oc} increases linearly with the area i.e. number of matrices of FCP.

II. Output performance depending on the magnitude of the force

It is plausible that the magnitude of the force applied onto the AL influences in the quantinty of polaronic influence that neigbouring polymeric chains exerts onto each other. The more force applied to the AL, the more the polymer strucutre will be deformated vertically and consequently the higher the electron density will be in the pressurized area. This will allow for more electrons hopping through the polymer networks to the metal/polymer interface region and afterwards translocating to the metal electrode. To have an idea of the magnitude of the force employed a set up involving a force sensor and a programmed arduino board was put into place (**Figure 3.3.3**). In **Figure 3.3.4 (a)** it is shown that the higher the force,

the higher the output voltage is. Altough little change is seen from 1 N to 4 N, with V_{oc} values between 10-12.5V, there are very significant increases in the voltage output for higher force magnitude. For an applied force of 8 N it has been seen that the average V_{oc} has risen to values between 20-30V, at 12 N the average output voltage ranges from 60-70V and, for force values of 16 N, the voltage rises to values between 70-80V. The phenomenon indicates that there is a threshold force impact after which the amount of charge transmutation increases rapidly. From 4N to 12N the voltage peaks increase six times. After that, increasing the force up to 16N results in an icrease of V_{oc}. It is obvious that the charge transfer mechanism, which completely depends on the mechanical-stimulus effect on polymeric chains, will be prominently dependent on the applied force. The average force impact that can be employed through hand patting was tested to be around 16N in average. The measurement was done several times by an average male human hand (70 kg weight, 175 cm height). The average force impact that can be employed through hand patting in general by a human with these characteristics was tested. Results are shown in the Annexes section, **Figure A.4.2**) For the force measurements the same electrode was used in the CCL (Cu), as well as same tapping frequency (16 Hz) and same size AL (2x3).

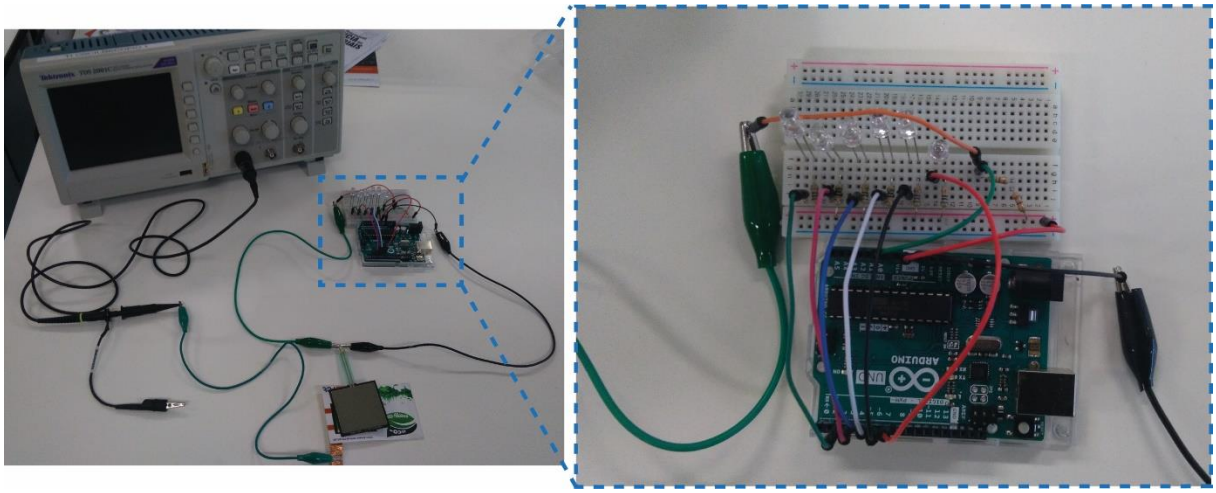

Figure 3.3.3 – Set-up for the force magnitude measurement including a close-up snapshot of the arduíno circuit

III. Output performance depending on the frequency of the force

At the metal/polymer interface there is an increase of charge density that will result in Fermi-level pinning and consequent translocation of electrons to the metallic structure. In the metal/polymer interface there will be metastable energy state through which, mechanically excited charge carriers from the polymer network, translocated to the Fermi energy level of metal. Now after releasing of mechanical stress, possibly few charges remain in these metastable energy levels, not successfully completing the translocation process. At a lower force frequency rate, these metastable charges have enough time to resettle to the polymer's Fermi energy level (which is most preferable ground state) again. And hence, for next mechanical stress application, all the charge carriers need energy to move from polymer's Fermi energy level for translocation. But if the frequency rate is faster, those charges, which stay in those metastable energy levels, will require less energy to initiate another charge translocation process, resulting in more carrier's translocation. Since the designed protype is for human-interactive applications, the maximum values of human tapping frequencies obtained, which is around 6 Hz, were used as maximum operating force frequency for eco-current harvesting measuring system. In Figure 3.3.4 (b) shows the V_{oc} under working frequencies, from 1 to 6 Hz, when the applied force is kept fixed at 16 N. It can be observed that V_{oc} remained very much the same for frequencies of 4 Hz, 5 Hz and 6 Hz (values averaged between 70-80 V). There is a slight decrease of V_{oc} below the frequencies of 3 Hz, with average values between 60-70V. For frequencies of 1 Hz and 2 Hz the average voltage output ranged from 50-60V. Although the variation of V_{oc} is not as prominent as for the applied force, it can be inferred that higher frequencies could presumably make faster the duration of the charge transfer

process, and consequently enhancing the output voltage values. In the frequency measurements the same electrode was used in the CCL (Cu), as well as same force magnitude and same size AL (2x3). (**Figure 3.3.4(b)**)

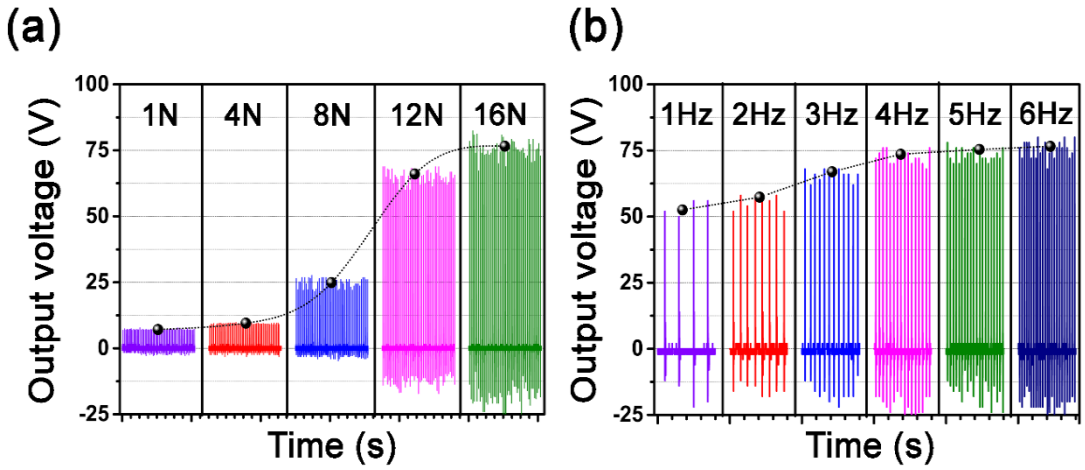

Figure 3.3.4 – Exhibited of the output voltage of the "eco-energy smart card" influenced by **(a)** the magnitude of force and **(b)** the frequency. In Annex section there is a real-time video (SV1) demonstrating the effect of both frequency and force.

IV. Output performance depending on the electrodes used as the CCL

The kind of electrode used has a big influence on the output voltage, since the main factor that comes into play in the charge transfer mechanism is the band alignment at the metal/polymer interface. Different metals equal different Fermi levels and consequently alters the ease with which electrons jump onto the energy band levels of the metal from the polymer. In order to further understand how this phenomenon influences the device's output several devices with different electrodes were built. Each "eco-energy" smart card was built with 2 × 3 matrices of FCP (i.e active layer) combined with gold (Device Name: D_{Au}), carbon (Device Name: D_C), copper (Device Name: D_{Cu}), silver (Device Name: D_{Ag}) and aluminum (Device Name: D_{Al}) electrode layer (i.e charge collector layer). In **Figure 3.3.5 (a)** and **3.3.5 (b)**, it is shown the output voltage for V_{oc} and output current, $I_{sc,}$ respectively, for all the devices.

The V_{oc} measurements were done just with the help of an oscilloscope. Whereas, the I_{sc} measurements were made by adding a 10 MΩ load resistance and a 100 Ω resistance in series. From the figure, it can be seen that devices with different electrodes in the CCL have different average values for both V_{oc} and I_{sc}. The tendency of voltage output is as follows: $D_{Ag} > D_{Cu} > D_C > D_{Au} > D_{Al}$. Notably, V_{oc} and I_{sc}, are maximum for the D_{Ag} (91V, 12 µA), followed closely by the D_{Cu} (80 V and 8.5 µA).

As expected, the Fermi level of the electrode plays a big role in the device's performance. When two metals or semiconductors with different work functions Φ_1 and Φ_2 (work necessary to bring an electron from the Femi level to vacuum) are connected, the material which has the higher φ will acquire a positive charge with respect to the other at the area of a contact, resulting in a contact potential difference (CPD). In order to estimate the work function difference (ΔΦ) between the CCL and the AL, the measurements were preformed using the Kelvin Probe Force Microscopy (KPFM) for all the electrode materials and FCP. KPFM is purely a surface probing technique. There is a necessity to perform a first pass to acquire topography information in tapping mode, the second pass has the cantilever at a determined height with an applied external DC-nulling voltage, so that a direct quantifiable analyses of the contact potential difference between the cantilever and the sample can be calculated.

$$CPD\ (V) = (\Phi_{probe} - \Phi_{sample}) / e \qquad (2)$$

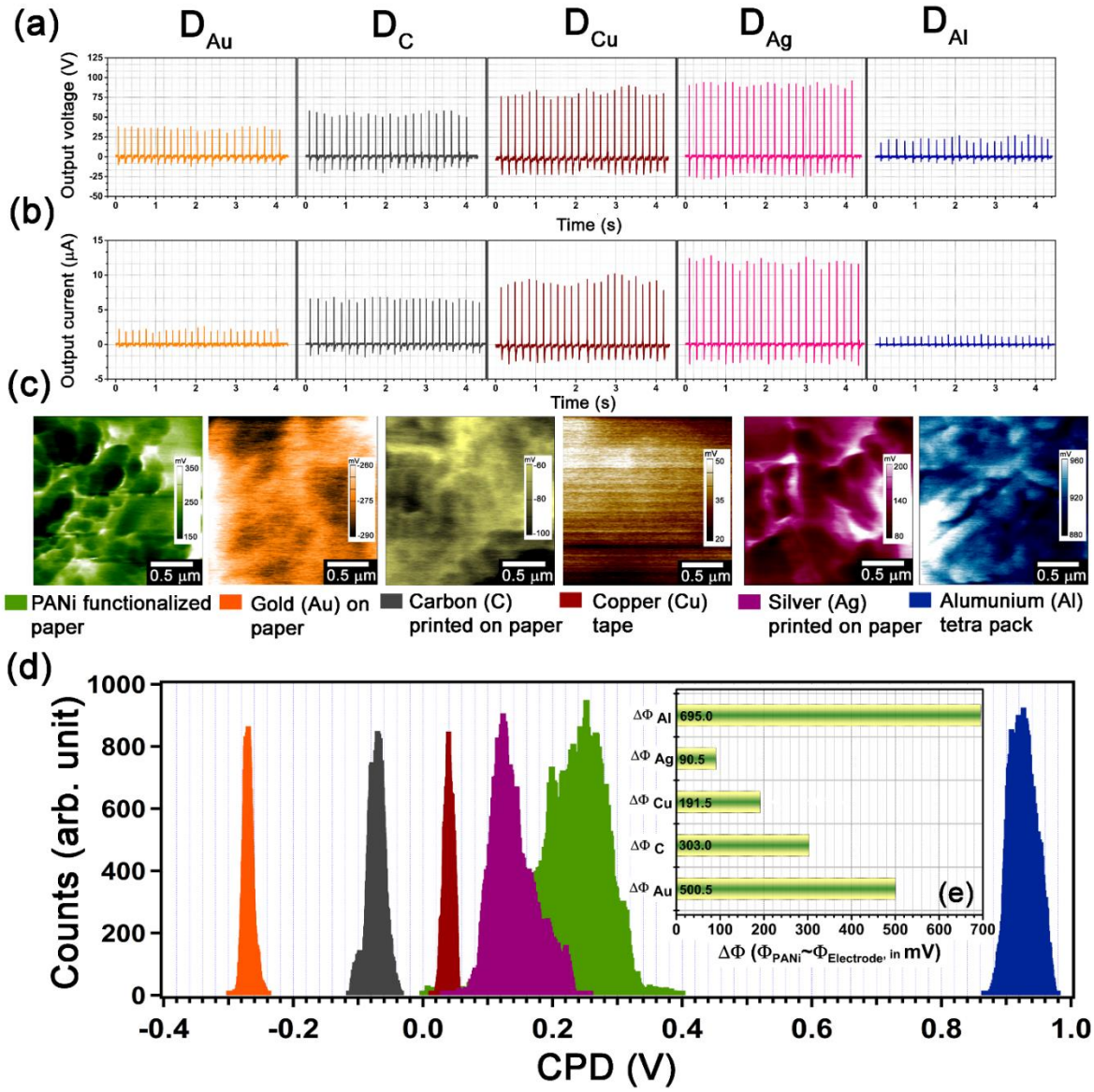

Figure 3.3.5 –The mechano-responsive spontaneous output electrical power obtained from different devices based on different metal electrodes, used in the charge collector layer (CCL): gold (D_{Au}), carbon (D_C), copper (D_{Cu}), silver (D_{Ag}) and aluminum (D_{Al}). **(a) (b**) Shows mechano-responsive output voltage and current, respectively for different devices using same applied force impact and frequencies. **(c)** Shows surface potential map by KPFM for different CCL (with different electrode materials) including AL (FCP). **(d)** The corresponding histogram distribution shows the mean of contact potential difference (CPD) for each material. **(e)** A schematic (not in scale) energy diagram based on mechano-stimuli charge transfer mechanism between CCL-AL is illustrated.

The work function difference ($\Delta\Phi$) will be inferred from calculating the difference between the average CPD of the FCP (CPD_{FCP}) and the average CPD of each CCL ($CPD_{CCL.}$). **Figure 3.3.5(c)** shows the KPFM mapping of the CPD in both the PANi and each electrode. Furthermore, a corresponding histogram profile (**Figure 3.3.5 (d)**) was added in order to make a better comparison between the values obtained for the CPD of all the materials. The average values of CPD from the histogram (**Figure 3.3.5(e)**) were used to calculate the $\Delta\Phi$ between PANi and each of the electrodes. When it comes to A_g, its interface with PANi was calculated to be $\Delta\Phi_{PANi/Ag}$ = 90 mV, which was determined to be the lowest value. The highest $\Delta\Phi$ value was determined to be the interface with aluminum, $\Delta\Phi_{PANi/Al}$= 900mV. In between are the values calculated for the rest of the materials $\Delta\Phi_{PANi\,/\,Cu}$ = 190 mV, $\Delta\Phi_{PANi\,/\,C}$ = 300 mV and $\Delta\Phi_{PANi\,/\,Au}$ = 700 mV. This matches well with the results obtained for the output voltages V_{oc} and the output current I_{sc}. The lower the work function between PANi and the device's electrode, the higher

the output voltage and current obtained from the mechanical stress applied. Indeed, Ag shows the higher electrical output performance and the lower work function values, in reverse Al shows the worst electrical output performance and the higher work function values. The same behavior is verified with the rest of the electrode materials.

It is worth noticing that the higher the work function difference between FCP and the electrodes, the higher the electronic density (at the interface) needs to be, in order to initiate a charge translocation. Consequently, for the same magnitude of applied force, fewer charge carriers are transferred to the CCL and therefore the lower the output performance of the device will be. A schematic for better understanding is illustrated in **Figure 3.3.6**

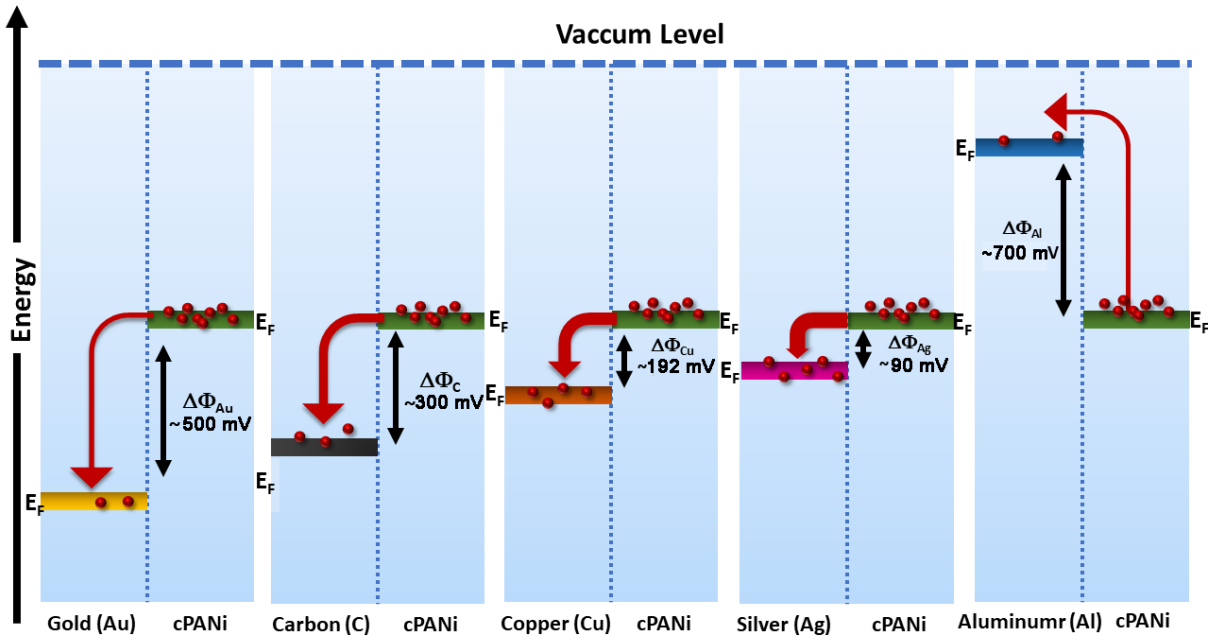

Figure 3.3.6 – A schematic (not in scale) of the energy diagram at the interface between the AL (PANi/cellulose composite system) and the CCL (paper-based electrode system).

A real-time video of touch-interactive energy harvesting from self-powered "eco-energy smart card" can be watched at https://drive.google.com/file/d/1cL2_zkrdDHPvP3s2WEnZcLB31-XHmV7N/view?usp=sharing (SV1).

3.4 "Eco-Energy Smart Card" Real-Field Applications

The practical applications of any electrical device are very much related to its power. The energy harvested mechanically from the device has an AC characteristic, so a rectifier was added to get a DC output signal. In **Figure 3.4.1** it is shown the spontaneous rectified output voltage for a typical device (D_{Ag}). The power density was calculated by adding in series resistors to a rectifier circuit (see in Annex section **Figure A.5.1**), whose values varied from 55 kΩ to 150 MΩ. In this way the power output can be calculated, $P = I^2 \times R$, from the average output voltage associated to each series resistance. Both the current and power densiy curves are shown in **Figure 3.4.2**.

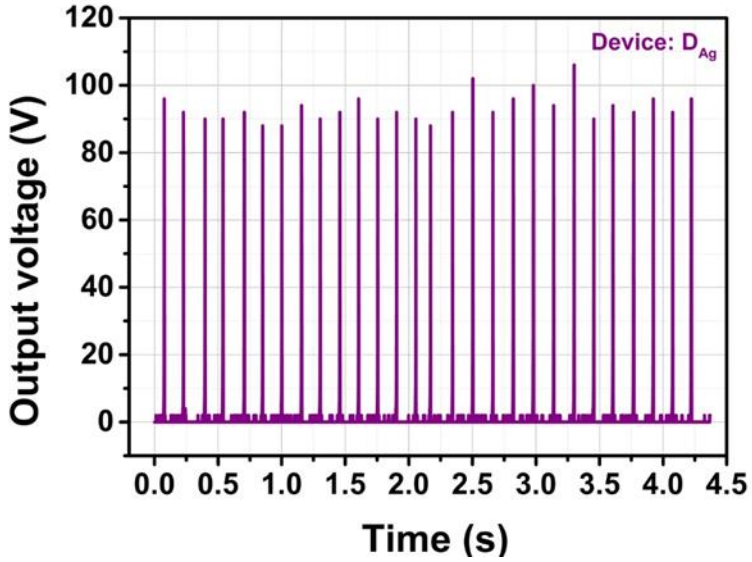

Figure 3.4.1 - DC Output voltage from device D_{Ag} with rectifying circuit

It is worth noticing once again that similarly to the V_{oc} and I_{sc} measurements the maximum power density (P_{max}) and current density (I_{max}) were both achieved by the device D_{Ag} ($P_{max/Ag}$ = 1.75 W m^{-2} and $I_{max/Ag}$ = 33.5 mA m^{-2}). The lowest values were obtained, also as expected by the aluminum device ($P_{max/Al}$ = 0.24 W m^{-2} and $I_{max/Al}$ = 12 mA m^{-2}). In between the values obtained for copper, carbon and gold were $P_{max/Cu}$ = 1.35 W m^{-2} and $I_{max/Cu}$ = 32.5 mA m^{-2}, $P_{max/C}$ = 0.7 W m^{-2} and $I_{max/C}$ = 22 mA m^{-2}, $P_{max/Au}$ = 0.26 W m^{-2} and $I_{max/Au}$= 15 mA m^{-2}, respectively. These results are aligned with the explanation provided above regarding the height of the energy barrier between FCP (AL) and the material of each electrode (CCL). A resume is shown in **Table 3.4.1**.

Table 3.4.1 - "Eco-Energy" Smart Card electrical characterization results for devices with different electrode material. D_{Cu} and D_{Ag} presented the best output performance

Device Name	Electrode Material	Work Function Difference Electrode/PANi (Δφ in mV)	Average V_{oc} (V)	Average I_{sc} (μA)	Maximum Power Density (W m^{-2})	Maximum Current Density (mA m^{-2})
D_{Au}	Gold	500	35.5	2	0.26	15
D_C	Carbon	303	54	6.5	0.7	22
D_{Cu}	Copper	191	80	8.5	1.35	32.5
D_{Ag}	Silver	90	91	12	1.75	33.5
D_{Al}	Aluminum	695	22	1	0.24	12

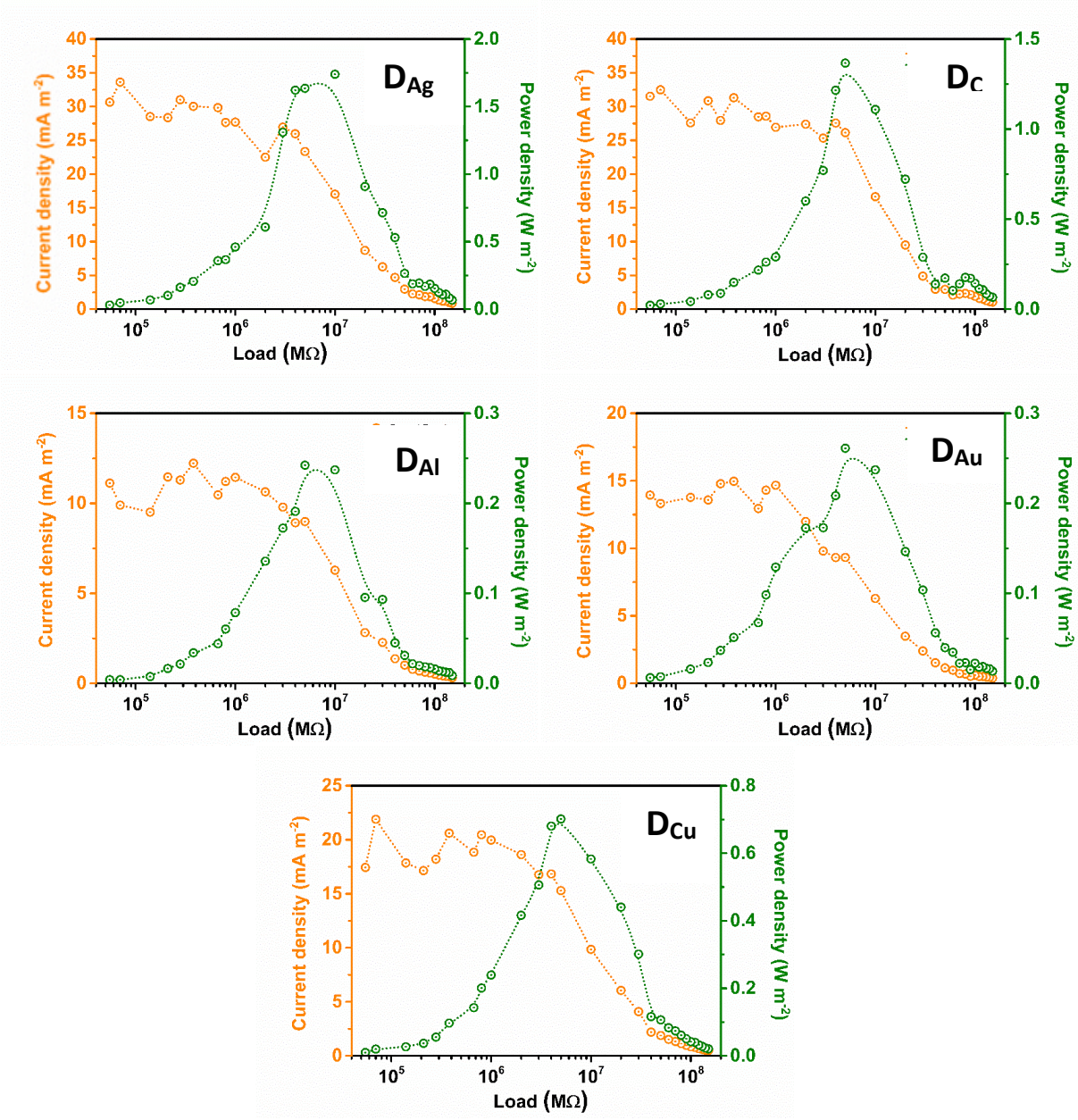

Figure 3.4.2 – Results obtained for the current density and power density curves for different devices using different materials in their CCL: silver (D_{Ag}); carbon (D_C); aluminum (D_{Al}); gold (D_{Au}) and copper (D_{Cu}). It can be observed that for lower the work function difference ($\Delta\Phi$) at the polymer/metal interface layer, the higher the maximum power and current density has been achieved.

The "eco-energy smart card", is able to instantaneously light up to 40 blue LEDs (20 mA rating, 5mm diameter and 8.6mm height) through patting. The LEDs were connected in series (**Figure 3.4.3 (a)** and **Figure 3.4.3 (c)**). It can also light up in parallel, five blue LEDs (**Figure 3.4.3 (b)**). The parallel configuration takes up more current to light up the LEDs, since this is a low power device it is expected that the parallel configuration does not light up as many LEDs. Five white LEDs were also light up in series configuration (see in Annexes **Figure A.5.2**).

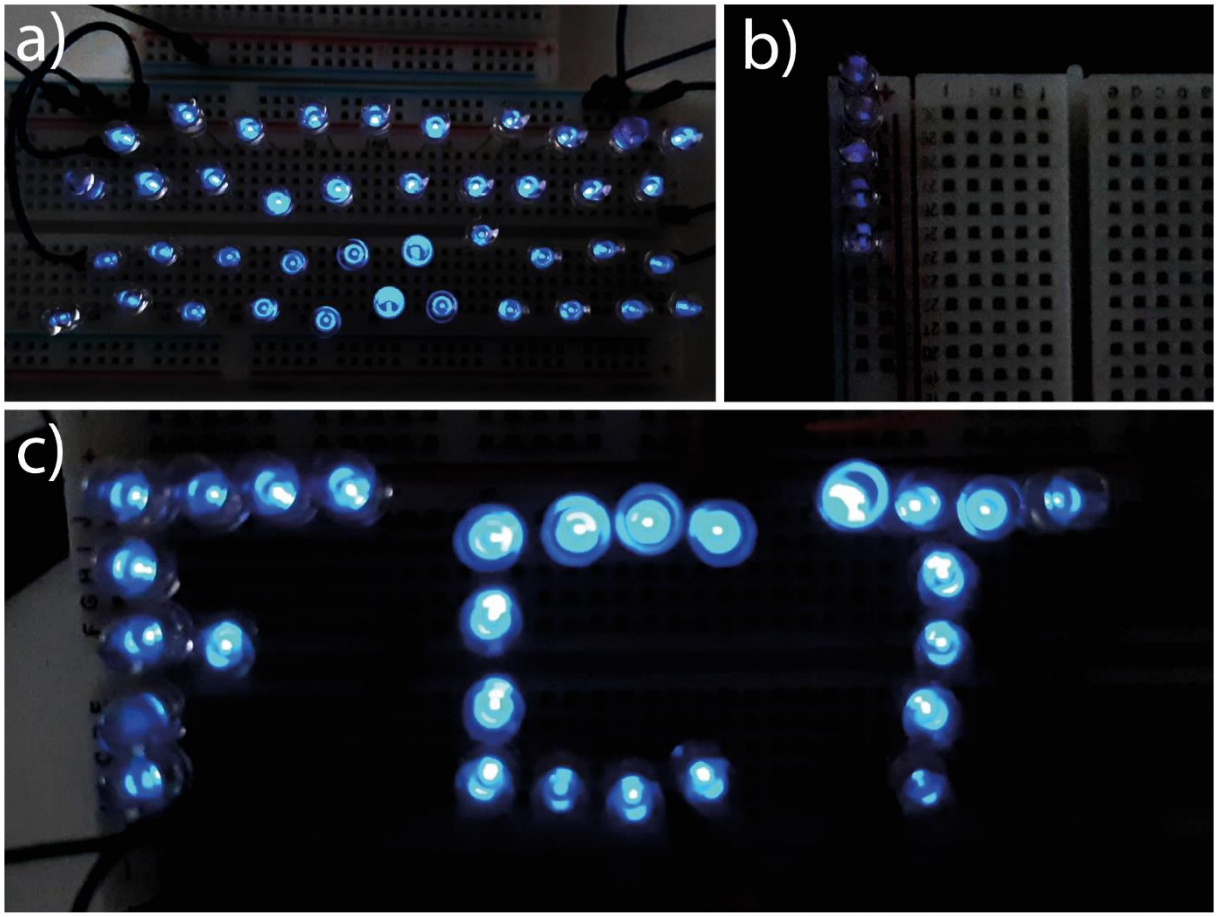

Figure 3.4.3 – Snapshot of LEDs lighting up during performance tests of the "eco-energy" smart card. Both in pictures **(a)** and **(c)** the LEDs are in series configuration. In figure **(b)** the LEDs are in parallel configuration. A real-time LED lighting up video demonstrating configuration **(a)** (SV2) and **(c)** (SV3) is also provided at:

https://drive.google.com/file/d/1N86oWoPspyAqdPscTTnuRqFMB481tcDr/view?usp=sharing (SV2)

https://drive.google.com/file/d/1Y1-f9KCnJCCzFmhFvmJ4RCt5O7_ysZqI/view?usp=sharing (SV3)

Similarly, to other tribo and piezoelectric power generation systems, this energy harvesting device is characterized by lower power yet high voltage output. In order to power up more sophisticated electronic equipment, it is necessary to charge up capacitors beforehand and then use that storage electrical energy to power that equipment. For that a capacitor with 10 µF capacitance was added in series to the rectifying circuit and tried to charge it with "eco-energy smart cards" using each type of electrode studied. In **Figure 3.4.4** there is a graphical representation of the amount of charge that the capacitor was able to harvest in a little more than 10 minutes.

Once again, similarly to the results presented above the "eco-energy" smart card the D_{Ag} and the D_{Cu} showed the best harvesting performance, while the aluminum and gold performed the most poorly. Moreover, the "eco-energy smart card" has been used for powering a portable humidity sensor by charging up a 47 µF commercial capacitor (47 µF) up to 2V. In **Figure 3.4.5** a snapshot of the humidity sensor that was powered up is presented. Also, the system setup and schematic of the rectifier circuit is shown.

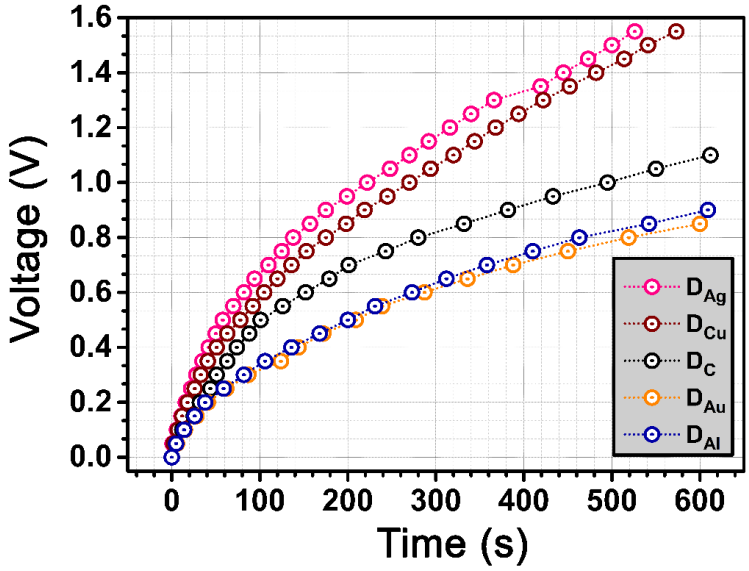

Figure 3.4.4 – Results obtained while charging up a commercial capacitor (10 µF) for different devices (D_{Ag}, D_{Cu}, D_C, D_{Au}, D_{Al}). The device D_{Ag} and the D_{Cu} were able to charge up to 1.5V in less than 10 minutes.

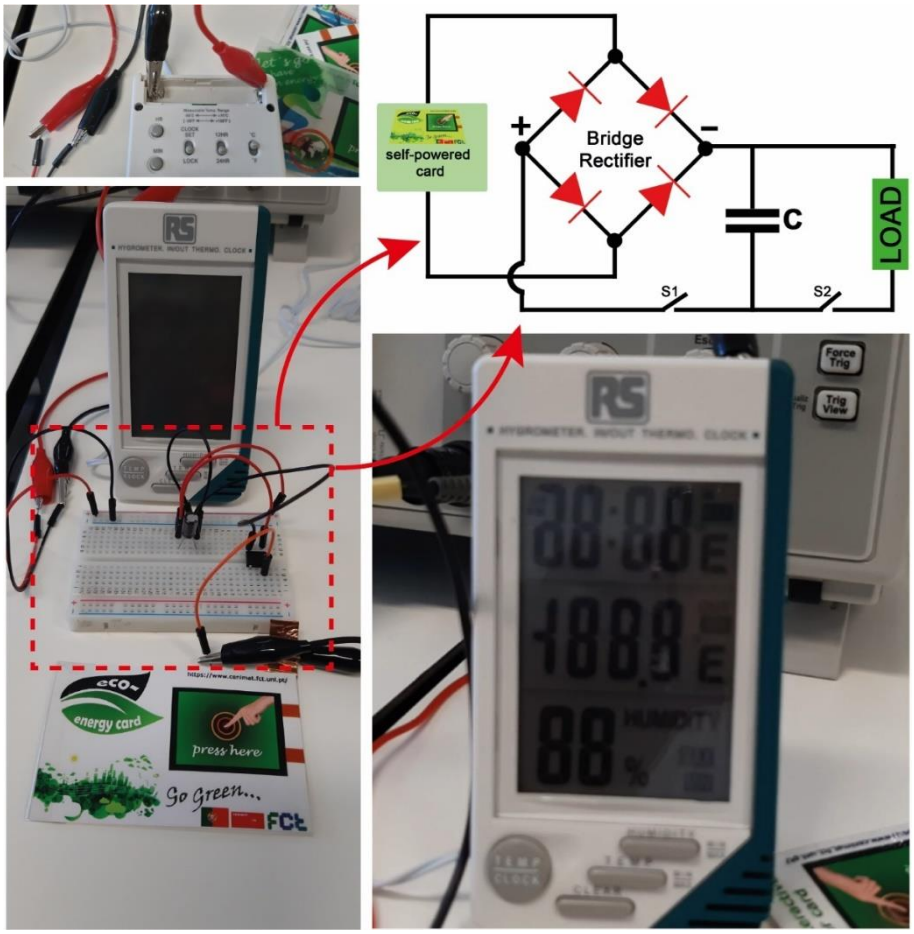

Figure 3.4.5 – Snapshot powering up a humidity sensor through charging up a commercial capacitor (47 µF). Also, the correspondent circuit diagram has been shown including schematic of rectifier circuit. A real-time video (SV4) of the humidity sensor, powering up can be consulted at:

https://drive.google.com/file/d/1r9LRNtKAzyNWx_5NfMsdjfQZIdyfsWXi/view?usp=sharing (SV4)

As a complementary test the output voltage was recorded in open circuit (V_{oc}) for 1200 cycles (**Figure 3.4.6**). The device remained very much stable and durable from the first cycles until the very last. The device used in this test was a D_{Ag}. The average V_{oc} values match the ones obtained above in the other tests for similar devices. Also, while charging up the capacitor, the devices were tapped at a frequency of 3-5Hz. In ten minutes, which was the time used for the capacitance test, the devices underwent 1800-3000 cycles. Several tapping tests were made in the course of six months, with relatively few changes in the electrical performance of the smart cards. It can be concluded that stability wise the prototypes can withstand a continuous use for human applications.

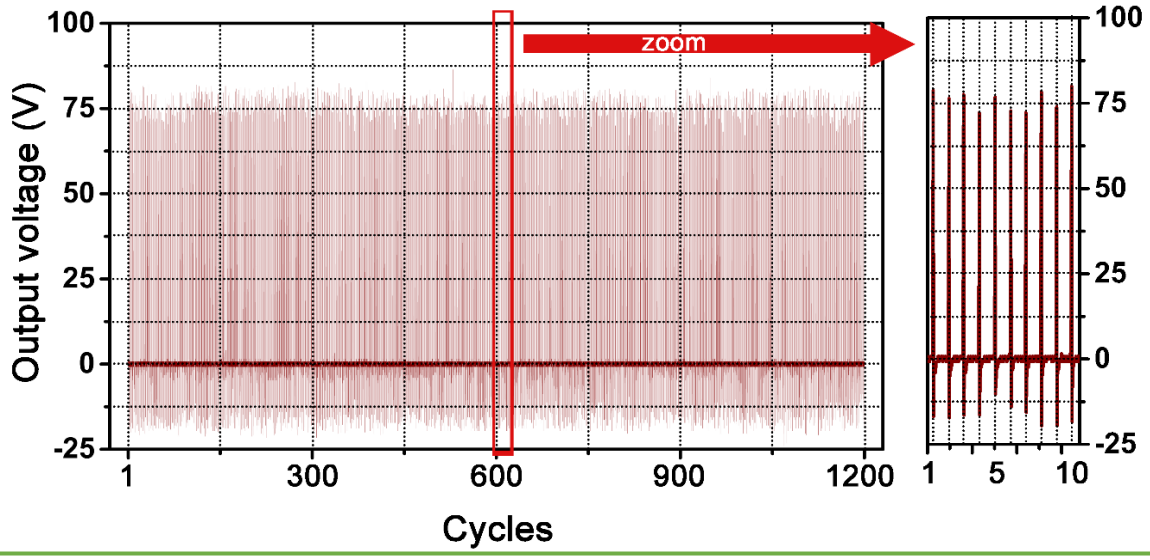

Figure 3.4.6 - "Eco-energy" smart card stability test; the device was put under a 1200 cycle of pressurized/non-pressurized states. There is no decrease in the output voltage during the test. In fact, the output voltage average remains mostly unchanged.

4. Conclusions and Future Perspectives

This work puts forward a novel concept of energy harvesting system, from which flexible, low-cost, and nearly "zero e-waste" "eco-energy smart card" were made. The devices made included mainly paper-based features which supports all the sustainable goals targeted. These devices can seize human mechanical dissipated energy and convert it into electrical energy.

In general, paper is not itself a material either for charge transporting abilities or charge generating. So, in order to attribute these characteristics to paper, it is functionalized with conductive polyaniline (PANi) through *in-situ* polymerization technique, empowering it for mechano-responsive energy harvesting abilities. The best conducting properties were found after the *in-situ* functionalization of WCP by a simple two-step drop casting method using aniline and its co-chemicals at room temperature. That shows very promising conductivity of the paper in the range of 0.1 S m^{-1}.

Furthermore, in this work, a prototyped energy harvesting device in the form of human-touch interactive "eco-energy smart cards" was designed, which is completely based on paper, so the "zero e-waste" challenge could be tackled. Devices were built having different kinds of metallic electrodes for CCL, namely: Ag (screen-printing), Al (Tetra pak™), Au (e-beam), C (screen-printing) and Cu (copper tape). It was verified that the more effective AL area onto which force is applied the higher is the electrical output. Also, electrode materials which had Fermi Energy levels closer to that of the PANi presented better electrical performance. For that several mechanical-stimuli electrical measurements were made as well as KPFM measurements for the Fermi-level value calculation.

The maximum power and current density that was achieved by our best device is 1.75 Wm^{-2} and 33.5 mA m^{-2}, respectively. This device was also able to light up 40 commercial blue LEDs and charging up a 47 µF capacitor, whose storage energy was then used to power a commercial humidity sensor. Robustness and durability of the eco-energy smart card has been tested for more than six months keeping all the devices in normal atmosphere.

Although very good results for the "eco-energy smart card" were obtained, further improvements can be made to the technology. Having that in mind, a lot of work has already been made during this thesis in order to improve this concept:

1. Active Layer:

    I. Other studies with respect to the AL have also been made, namely the use of a different conjugated polymer. Functionalization of the same WCP with Polypyrrole (PPy) was tried. Most bibliography suggests that PPy shows better conductivity than PANi. The preliminary results showed that indeed the conductivity of the FCP is better than the one obtained by using a PANi matrix, the best value obtained was 36 Ω of lateral resistance, (values are usually not higher than 200 Ω). The devices using PPy functionalized chromatography paper present a slight output performance improvement from its PANi competitors, but less stability. The active layer deteriorates faster after some tapping. Further studies are being conducted in order to improve PPy's mechanical stability without compromising its electrical performance.

    II. Improving the electrical performance of the PANi active layer is also a possibility. If the reactions temperature is reduced, it is expected that the electrical conductivity of the polymer improves due low reactions kinetics which would likely result in better polymerization and chain formation.

    III. The influence of the PANi microstructures, in the FCP, on the output performance of the "eco-energy smart card" has to be taken into consideration. The granular structure was the one mostly used in the AL. Other microstructures, like nanowires or nano-rods, can be studied to see the impact that this will have in the device's performance.

2. Charge Collector Layer:

    I. The effect of the electrode material crystallinity also affects the final output of the device. Some preliminary results showed that paper-based electrodes with e-beam deposited copper showed better output values than its tape counterpart. Further studies need to be made considering, the crystallinity phase of the metallic electrodes. The output values of $D_{Cu(e\text{-}beam)}$ surpassed even the ones obtained with the D_{Ag}. The C_u microstructure is different in both cases. It is therefore necessary to make further investigation in the nanostructure of the electrodes, whether its nanoparticles, nanowires, etc. The difference in Fermi level also depends on the crystallinity of the electrode. If the Fermi level changes, so does the ease that charge carriers translocate to the CCL, which would improve the performance of the "eco-energy smart card".

3. Expanding the charge transfer mechanism concept:

    I. The charge transfer mechanism concept applied to the "eco-energy smart card" is based on energy harvesting of human mechanical energy. Fortunately, there are a lot of sources of mechanical energy. It is our objective to project prototypes that allow for conversion of energy from several other sources.

    II. The concept has also room for improvement especially if developed as an all printed based device. All printed paper technologies are cheaper greener and trending which could also potentially give rise to a growth in the printed electronics industry.

    III. The technology has tremendous potential in other microelectronic applications. If coupled with flexible paper-based supercapacitors, the technology could maybe be able to power up more complex electronic equipment and thus making the way to "real-field" industrial applications. They can also be applicable for other technologies such as sensors and wireless systems, for example in tracking applications that could trace someone's movement while walking.

5. References

[1] World Electronic Waste Problem, https://time.com/5594380/world-electronic-waste-problem/

[2] E-Waste Monitor: http://ewastemonitor.info

[3] The World's Worst Electronic Waste Offenders Infographic: https://www.forbes.com/sites/niallmccarthy/2019/02/27/the-worlds-worst-electronic-waste-offenders-infographic/#16ee54792097

[4] Baldé, C.P., Forti V., Gray, V., Kuehr, R., Stegmann,P. : The Global E-waste Monitor – 2017, United Nations University (UNU), International Telecommunication Union (ITU) & International Solid Waste Association (ISWA), Bonn/Geneva/Vienna

[5] A New Circular Vision for Electronics (Time for a Global Reboot) - http://www3.weforum.org/docs/WEF_A_New_Circular_Vision_for_Electronics.pdf

[6] Eurostat, Waste Statistics: https://ec.europa.eu/eurostat/statistics-explained/index.php/Waste_statistics

[7] Circular Economy Definition Importance and Benefits: http://www.europarl.europa.eu/news/en/headlines/economy/20151201STO05603/circular-economy-definition-importance-and-benefits

[8] Hu, S., Rajamani, R., & Yu, X. (2012). Flexible solid-state paper-based carbon nanotube supercapacitor. Applied Physics Letters, 100(10), 104103.

[9] Li, K., Liu, X., Chen, S., Pan, W., & Zhang, J. (2018). A flexible solid-state supercapacitor based on graphene/polyaniline paper electrodes. Journal of Energy Chemistry

[10] Fortunato, E., Correia, N., Barquinha, P., Costa, C., Pereira, L., Gonçalves, G., & Martins, R. (2009). Paper field effect transistor. Zinc Oxide Materials and Devices IV. doi: 10.1117/12.816547

[11] Martins, R., Gaspar, D., Mendes, M. J., Pereira, L., Martins, J., Bahubalindruni, P., Barquinha, P., Fortunato, E. (2018). Papertronics: Multigate paper transistor for multifunction applications. Applied Materials Today, 12, 402–414. doi: 10.1016/j.apmt.2018.07.002

[12] Oliveira, R. A., Camargo, F., Pesquero, N. C., & Faria, R. C. (2017). A simple method to produce 2D and 3D microfluidic paper-based analytical devices for clinical analysis. Analytica Chimica Acta, 957, 40-46

[13] S. Parandeh, M. Kharaziha, F. Karimzadeh, "An eco-friendly triboelectric hybrid nanogenerators based on graphene oxide incorporated polycaprolactone fibers and cellulose paper", Nano Energy 59 (2019) 412-21.

[14] Hu, L., & Cui, Y. (2012). Energy and environmental nanotechnology in conductive paper and textiles. Energy & Environmental Science, 5(4), 6423. doi: 10.1039/c2ee02414d

[15] H. Guo, M. H. Yeh, Y. C. Lai, Y. Zi, C. Wu, Z. Wen, C. Hu, Z. L. Wang, "All-in-One Shape-Adaptive Self-Charging Power Package for Wearable Electronics", ACS Nano 10 (2016) 10580−8.

[16] E-paper Display market Size: https://www.maximizemarketresearch.com/market-report/global-e-paper-display-market/8353/

[17] Paper's role in circular economy: https://www.australianpaper.com.au/environment/circular-economy/

[18] Deng, X.-Y. (2011). Light-Emitting Devices with Conjugated Polymers. International Journal of Molecular Sciences, 12(3), 1575–1594. doi: 10.3390/ijms12031575

[19] Santos, L. F., & Gozzi, G. (2016). Electrical Properties of Polymer Light-Emitting Devices. Conducting Polymers. doi: 10.5772/64358

[20] Han, L. Dai, “Conducting Polymers for Flexible Supercapacitors”, Macromol. Chem. Phys. 220 (2019) 1800355.

[21] H. Wang, M. Barrett, B. Duane, J. Gu, F. Zenhausern, “Materials and processing of polymer-based electrochromic devices”, Mater. Sci. Eng., B 228 (2018) 167-74.

[22] Amer, K., Ebrahim, S., Feteha, M., Soliman, M., & El-Shaer, A. (2017). Organic field effect transistor based on polyaniline - dodecylbenzene sulphonic acid for humidity sensor. 2017 34th National Radio Science Conference (NRSC). doi: 10.1109/nrsc.2017.7893514

[23] Bufon, C. C. B., & Heinzel, T. (2006). Polypyrrole thin-film field-effect transistor. Applied Physics Letters, 89(1), 012104. doi: 10.1063/1.2219375

[24] C. Della Pina et al., "Towards “Green” Smart Materials for Force and Strain Sensors: The Case of Polyaniline", Key Engineering Materials, Vol. 644, pp. 157-162, 2015

[25] Patni, N., Jain, N., & Pillai, S. G. (2017). Polyaniline-Based Sensors for Monitoring and Detection of Ammonia and Carbon Monoxide Gases. Trends and Applications in Advanced Polymeric Materials, 145–162. doi: 10.1002/9781119364795.ch8

[26] Kim, Y.-H., Kim, M., Oh, S., Jung, H., Kim, Y., Yoon, T.-S., … Lee, H. H. (2012). Organic memory device with polyaniline nanoparticles embedded as charging elements. Applied Physics Letters, 100(16), 163301. doi: 10.1063/1.4704571

[27] Goswami, S., Nandy, S., Calmeiro, T., Igreja, R., Martins, R. and Fortunato, E. (2016). Stress Induced Mechano-electrical Writing-Reading of Polymer Film Powered by Contact Electrification Mechanism. Scientific Reports, 6(1).

[28] Baik, K., Park, S., Yun, C., & Park, C. H. (2019). Integration of Polypyrrole Electrode into Piezoelectric PVDF Energy Harvester with Improved Adhesion and Over-Oxidation Resistance. Polymers, 11(6), 1071. doi: 10.3390/polym11061071

[29] Wang, H., Lin, J., & Shen, Z. X. (2016). Polyaniline (PANi) based electrode materials for energy storage and conversion. Journal of Science: Advanced Materials and Devices, 1(3), 225-255.

[30] Goswami, S., Santos, A. D., Nandy, S., Igreja, R., Barquinha, P., Martins, R., & Fortunato, E. (2019). Human-motion interactive energy harvester based on polyaniline functionalized textile fibers following metal/polymer mechano-responsive charge transfer mechanism. Nano Energy, 60, 794–801. doi: 10.1016/j.nanoen.2019.04.012

[31] Goswami, S., Nandy, S., Banerjee, A. N., Kiazadeh, A., Dillip, G. R., Pinto, J. V., Joo, S. W., Martins, R., Fortunato, E. (2017). “Electro-Typing” on a Carbon-Nanoparticles-Filled Polymeric Film using Conducting Atomic Force Microscopy. Advanced Materials, 29(47), 1703079

[32] Youssef, A., Kamel, S., El-Sakhawy, M., & Samahy, M. E. (2012). Structural and electrical properties of paper–polyaniline composite. Carbohydrate Polymers, 90(2), 1003- 1007.

[33] Global renewable energy consumption: https://ourworldindata.org/renewable-energy

[34] Renewable Energy Investment Market 2019-2026: https://www.marketexpert24.com/2019/10/01/impressive-growth-for-renewable-energy-investment-market-2019-26-latest-quality-informative-study-focusing-key-players-huawei-investment-holding-co-ltd-abb-ltd-jiangsu-goodwe-power-s/

[34] Riddick, R. and Kuo, A. (2016). Soft tissues store and return mechanical energy in human running. Journal of Biomechanics, 49(3), pp.436-441.

[35] Priya, S. (2005). Modeling of electric energy harvesting using piezoelectric windmill. Applied Physics Letters, 87(18), p.184101

[36] Wang, Y., Duan, J., Zhao, Y., He, B. and Tang, Q. (2018). Harvest rain energy by polyaniline-graphene composite films. Renewable Energy, 125, pp.995-1002.

[37] Haque, R., Chandran, O., Lani, S. and Briand, D. (2018). Self-powered triboelectric touch sensor made of 3D printed materials. Nano Energy, 52, pp.54-62.

[38] Wang, Z. L., & Wang, A. C. (2019). On the origin of contact-electrification. Materials Today. doi: 10.1016/j.mattod.2019.05.016

[39] Guldiken, R., and O. Onen. "MEMS Ultrasonic Transducers for Biomedical Applications." MEMS for Biomedical Applications, 2012, pp. 120–149., doi:10.1533/9780857096272.2.120.

[40] Arnau, A., & Soares, D. Fundamentals of Piezoelectricity. Piezoelectric Transducers And Applications, 1-38. doi: 10.1007/978-3-540-77508-9_1

[41] Pan, Shuaihang, and Zhinan Zhang. "Fundamental Theories and Basic Principles of Triboelectric Effect: A Review." Friction, vol. 7, no. 1, 2018, pp. 2–17., doi:10.1007/s40544-018-0217-7.

[42] Niu, Simiao, and Zhong Lin Wang. "Theoretical Systems of Triboelectric Nanogenerators." Nano Energy, vol. 14, 2015, pp. 161–192., doi:10.1016/j.nanoen.2014.11.034.

[43] Wang, Zhong Lin, et al. "Triboelectrification." Triboelectric Nanogenerators Green Energy and Technology, 2016, pp. 1–19., doi:10.1007/978-3-319-40039-6_1.

[44] Kumar, A., Kiran, R., Chauhan, V. S., Kumar, R., & Vaish, R. (2018). Piezoelectric energy harvester for pacemaker application: a comparative study. Materials Research Express, 5(7), 075701. doi: 10.1088/2053-1591/aab456

[45] Lim, G. B. (2019). Pacemaker powered by cardiac motion. Nature Reviews Cardiology, 16(7), 386–386. doi: 10.1038/s41569-019-0208-z

[46] Bowen, C. R., & Arafa, M. H. (2014). Energy Harvesting Technologies for Tire Pressure Monitoring Systems. Advanced Energy Materials, 5(7), 1401787. doi: 10.1002/aenm.201401787

[47] Blažević, D., Kamenar, E., & Zelenika, S. (2013). Load optimised piezoelectric generator for powering battery-less TPMS. Smart Sensors, Actuators, and MEMS VI. doi: 10.1117/12.2016870

[48] Kim, K.-B., Cho, J. Y., Jabbar, H., Ahn, J. H., Hong, S. D., Woo, S. B., & Sung, T. H. (2018). Optimized composite piezoelectric energy harvesting floor tile for smart home energy management. Energy Conversion and Management, 171, 31–37. doi: 10.1016/j.enconman.2018.05.031

[49] Ricquebourg, V., Menga, D., Durand, D.,Marhic, B., Delahoche, L., and Loge, C. The smart home concept: our immediate future.in E-Learning in Industrial Electronics, 20061ST IEEE International Conference on.2006. IEEE.

[50] Li, X., & Sun, Y. (2017). WearETE: A Scalable Wearable E-Textile Triboelectric Energy Harvesting System for Human Motion Scavenging. Sensors, 17(11), 2649. doi: 10.3390/s17112649

[51] Turkmen, A. C., & Celik, C. (2018). Energy harvesting with the piezoelectric material integrated shoe. Energy, 150, 556–564. doi: 10.1016/j.energy.2017.12.159

[52] Mokhtari, F., Foroughi, J., Zheng, T., Cheng, Z., & Spinks, G. M. (2019). Triaxial braided piezo fiber energy harvesters for self-powered wearable technologies. Journal of Materials Chemistry A, 7(14), 8245–8257. doi: 10.1039/c8ta10964h

[53] Wong, V. K., Ho, J. H., & Yap, E. H. (2014). Experimental Study of a Piezoelectric Rain Energy Harvester. Advanced Materials Research, 1043, 263–267. doi: 10.4028/www.scientific.net/amr.1043.263

[54] Oy, S. A., & Özdemir, A. E. (2017). Piezoelectric-Based Low-Power Wind Generator Design and Testing. Arabian Journal for Science and Engineering, 43(6), 2759–2767. doi: 10.1007/s13369-017-2799-1

[55] Yang, Y., Zhu, G., Zhang, H., Chen, J., Zhong, X., Lin, Z., Su, Y., Bai, P., Wen, X. and Wang, Z. (2013). Triboelectric Nanogenerator for Harvesting Wind Energy and as Self- Powered Wind Vector Sensor System. ACS Nano, 7(10), pp.9461-9468

[56] Saadatnia, Z., Asadi, E., Askari, H., Zu, J. and Esmailzadeh, E. (2017). Modeling and performance analysis of duck-shaped triboelectric and electromagnetic generators for water wave energy harvesting. International Journal of Energy Research, 41(14), pp.2392-2404.

[57] Sahatiya, P., Kannan, S. and Badhulika, S. (2018). Few layer MoS2 and in situ poled PVDF nanofibers on low cost paper substrate as high performance piezo-triboelectric hybrid nanogenerator: Energy harvesting from handwriting and human touch. Applied Materials Today, 13, pp.91-99.

[58] Xia, K., Zhu, Z., Zhang, H., Du, C., Xu, Z. and Wang, R. (2018). Painting a high-output triboelectric nanogenerator on paper for harvesting energy from human body motion. Nano Energy, 50, pp.571-580.

[59] Seol, M., Han, J., Moon, D. and Meyyappan, M. (2017). Triboelectric nanogenerator for Mars environment. Nano Energy, 39, pp.238-244.

[60] - Yang, P.-K., Lin, Z.-H., Pradel, K. C., Lin, L., Li, X., Wen, X., … Wang, Z. L. (2015). Paper-Based Origami Triboelectric Nanogenerators and Self-Powered Pressure Sensors. ACS Nano, 9(1), 901–907. doi: 10.1021/nn506631t

[61] - Yao, C., Hernandez, A., Yu, Y., Cai, Z., & Wang, X. (2016). Triboelectric nanogenerators and power-boards from cellulose nanofibrils and recycled materials. Nano Energy, 30, 103–108. doi: 10.1016/j.nanoen.2016.09.036

[62] Wu, Y., Luo, Y., Qu, J., Daoud, W. A., & Qi, T. (2019). Liquid single-electrode triboelectric nanogenerator based on graphene oxide dispersion for wearable electronics. Nano Energy, 64, 103948. doi: 10.1016/j.nanoen.2019.103948

[63] Cui, C., Wang, X., Yi, Z., Yang, B., Wang, X., Chen, X., … Yang, C. (2018). Flexible Single-Electrode Triboelectric Nanogenerator and Body Moving Sensor Based on Porous Na2CO3/Polydimethylsiloxane Film. ACS Applied Materials & Interfaces, 10(4), 3652–3659. doi: 10.1021/acsami.7b17585

[64] Sun, N., Wen, Z., Zhao, F., Yang, Y., Shao, H., Zhou, C., & Shen, Q. (2017). Nano Energy All fl exible electrospun papers based self-charging power system. Nano Energy, 38(May), 210–217.

[65] M., V. P., Pina, C. D., & Falletta, E. (2018). Polyaniline Blends, Composites, and Nanocomposites. Elsevier.

[66] Abu-Thabit, N. Y. (2016). Chemical Oxidative Polymerization of Polyaniline: A Practical Approach for Preparation of Smart Conductive Textiles. Journal of Chemical Education, 93(9), 1606–1611. doi: 10.1021/acs.jchemed.6b00060

[67] Nastase, F. (2019). Introductory Chapter: Polyaniline - From Synthesis to Practical Applications. Polyaniline - From Synthesis to Practical Applications [Working Title]. doi: 10.5772/intechopen.83397

[68] Bláha, M., Trchová, M., Bober, P., Morávková, Z., Prokeš, J., & Stejskal, J. (2017). Polyaniline: Aniline oxidation with strong and weak oxidants under various acidity. Materials Chemistry and Physics, 194, 206–218. doi: 10.1016/j.matchemphys.2017.03.028

[69] Sannigrahi, J., & Majumdar, S. (2013). Effect of HCl doping in polyaniline: Transport and optical studies. doi: 10.1063/1.4791349

[70] Macdiarmid, A., Chiang, J., Richter, A., & Epstein, A. (1987). Polyaniline: a new concept in conducting polymers. Synthetic Metals, 18(1-3), 285–290. doi: 10.1016/0379-6779(87)90893-9

[71] Macdiarmid, A. G., & Epstein, A. J. (1995). Secondary doping in polyaniline. Synthetic Metals, 69(1-3), 85–92. doi: 10.1016/0379-6779(94)02374-8

[72] Abdelraheem, A., El-Shazly, A., & Elkady, M. (2018). Characterization of atypical polyaniline nano-structures prepared via advanced techniques. Alexandria Engineering Journal, 57(4), 3291–3297. doi: 10.1016/j.aej.2018.01.012

[73] Bernard, M.-C., Bich, V. T., Torresi, S. C. D., & Goff, A. H.-L. (1997). Spectroelectrochemical characterization (OMA and Raman) of sulfonic acids — doped polyanilines. Synthetic Metals, 84(1-3), 785–786. doi: 10.1016/s0379-6779(96)04145-8

[74] Xu, Y., Dai, L., Chen, J., Gal, J., & Wu, H. (2007). Synthesis and characterization of aniline and aniline- o -sulfonic acid copolymers, 43, 2072–2079. https://doi.org/10.1016/j.eurpolymj.2006.09.017

[75] Sapurina, I., & Shishov, M. (2012). Oxidative Polymerization of Aniline: Molecular Synthesis of Polyaniline and the Formation of Supramolecular Structures. New Polymers for Special Applications. doi: 10.5772/48758

[76] Zhang, L., & Wan, M. (2002). Synthesis and characterization of self-assembled polyaniline nanotubes doped with D-10-camphorsulfonic acid. Nanotechnology, 13(6), 750–755. doi: 10.1088/0957-4484/13/6/311

[77] Sedenková, I., Trchová, M., Stejskal, J., & Bok, J. (2007). Polymerization of Aniline in the Solutions of Strong and Weak Acids: The Evolution of Infrared Spectra and Their Interpretation Using Factor Analysis. Applied Spectroscopy, 61(11), 1153–1162. doi: 10.1366/000370207782597058

[78] Zhang, X., Kolla, H. S., Wang, X., Raja, K., & Manohar, S. K. (2006). Fibrillar Growth in Polyaniline. Advanced Functional Materials, 16(9), 1145–1152. doi: 10.1002/adfm.200500478

[79] Park, H., Kim, T., Huh, J., Kang, M., Lee, J. E., Yoon, H., & Al, P. E. T. (2012). Anisotropic Growth Control of Polyaniline Nanostructures and Their Morphology-Dependent Electrochemical Characteristics, (9), 7624–7633.

[80] M. Trchová, Z. Morávková, M. Bláha, J. Stejskal "Raman spectroscopy of polyaniline and oligoaniline thin films", Electrochimica Acta 122 (2014) 28-38.

[81] M. C. Bernard, A. H. Goff, "Quantitative characterization of polyaniline films using Raman spectroscopy I: Polaron lattice and bipolaron", Electrochimica Acta 52 (2006) 595–603.

[82] Malvankar, N. S., Yalcin, S. E., Tuominen, M. T., & Lovley, D. R. (2014). Visualization of charge propagation along individual pili proteins using ambient electrostatic force microscopy. Nature Nanotechnology, 9(12), 1012–1017. doi: 10.1038/nnano.2014.236

[83] M. Nonnenmacher, M. P. O'Byle, and H.K. Wickramasinghe, Appl. Phys. Lett. **58**, 2921 (1991)

Annexes

Annex 1. – Materials and Methods

The "eco-energy smart cards" were built with an AL coupled with different types of electrodes and a protecting cover (standard size of 85.60 × 53.98 mm2), either hard paper or tracing. Inside each "eco-energy" smart card, 3×2 pixelated area of FCP has been used. Below, there is some additional schematic regarding the whole fabrication process of the devices **(Figure A.1.1**) and the several types of electrodes used (**Figure A.1.2**).

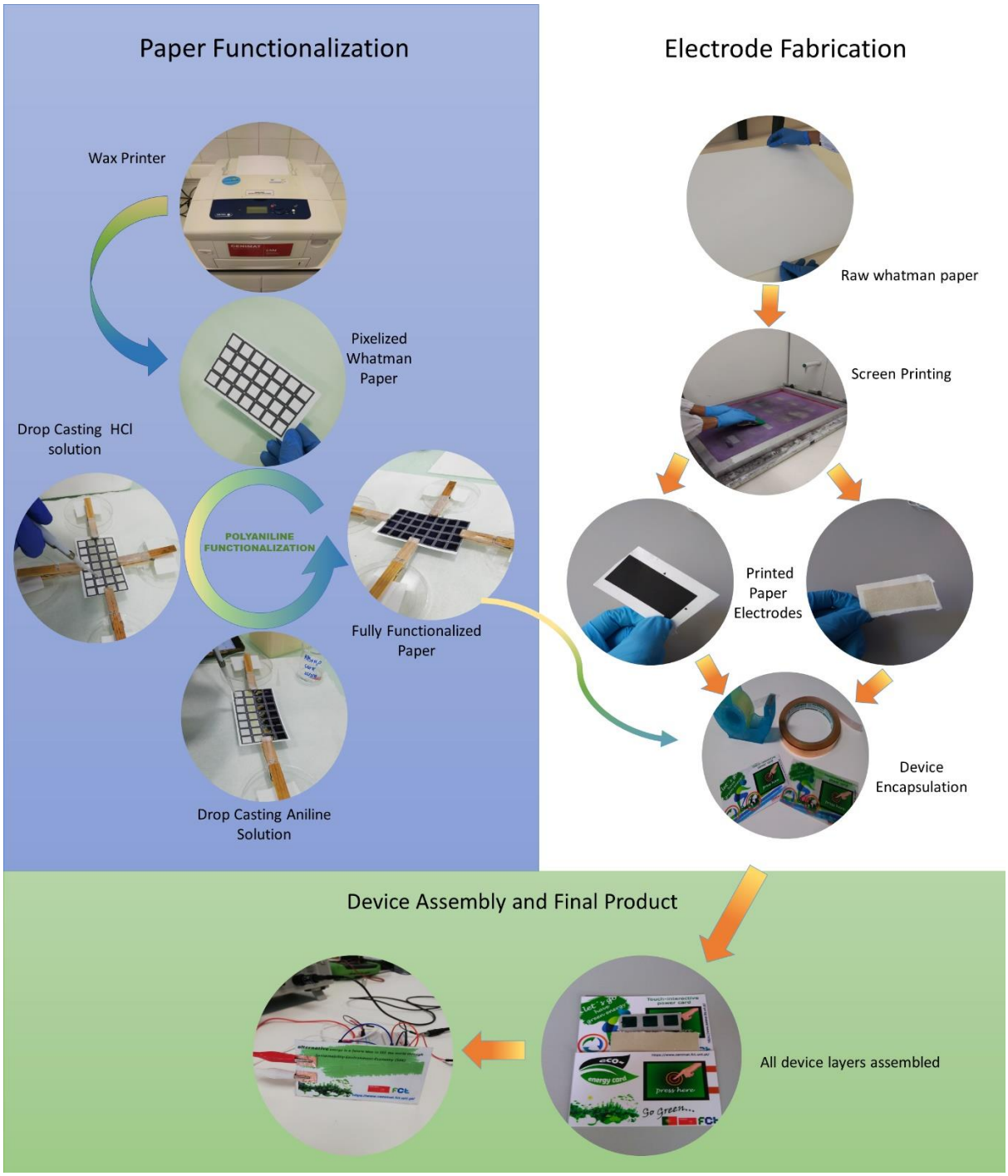

Figure A.1.1 – Layout of the fabrication process of the "eco-energy smart card", representing all of the processes from materials synthesis to fabrication. The whole manufacturing process from the raw paper until the final device is showed.

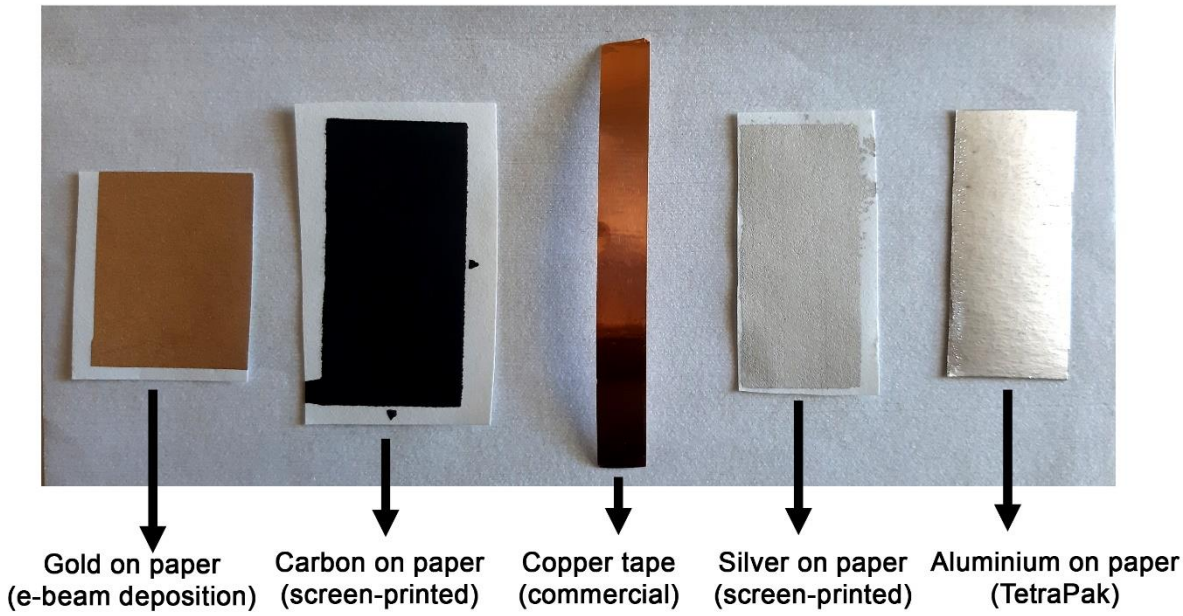

Figure A.1.2 - Different kinds of electrodes used as charge collector layer (CCL)

Annex 2. – Chemical and Morphology Analyses

A PANi/cellulose composite was synthesized, which would work as our active material for mechano-responsive charge transfer mechanism. This composite was made by the *in-situ* polymerization, drop-casting technique, which formed granular PANi in the paper's cellulose structure. In **Figure A.2.1** there is a FESEM image of raw paper (WCP) without functionalization.

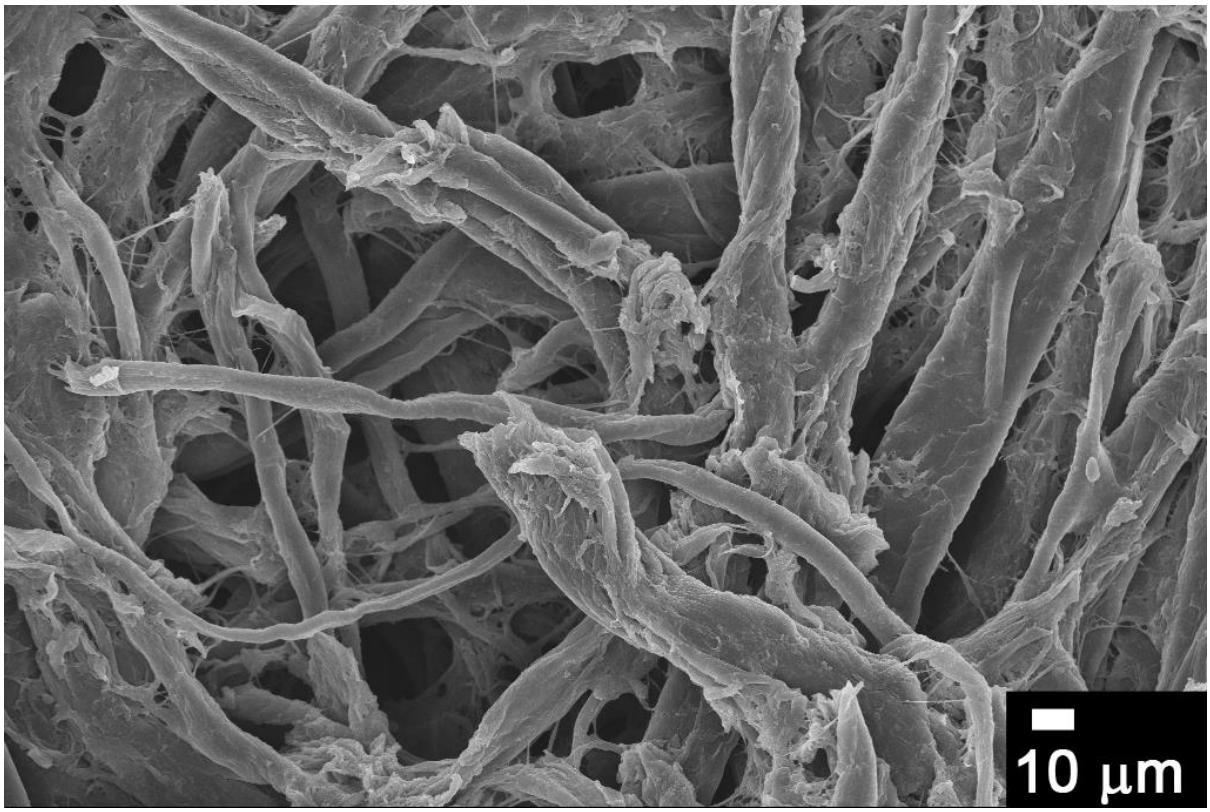

Figure A.2.1 – FESEM image of raw WCP.

Annex 3. – Electrical Analyses

The electrical properties of FCP were studied in order to understand the effectiveness of the polymerization process. Due to the presence of localized charges, the charge distribution pattern of raw WCP should be different form the FCP. For that the EFM technique was used to investigate the charge distribution of the samples. A schematic of the EFM technique is presented in **Figure A.3.1**

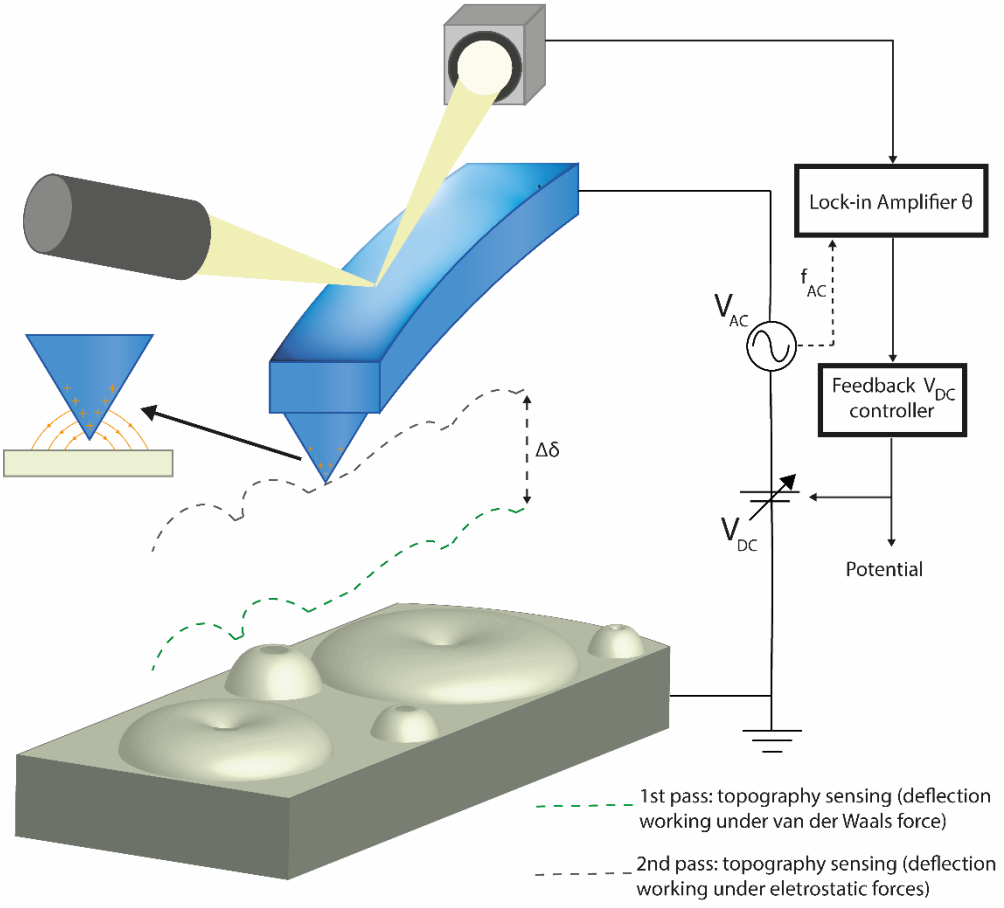

Figure A.3.1 - Schematic of the working principle of EFM

Annex 4. – "Eco-Energy Smart Card" Performance

In order to study the factors that influenced the output performance of the "eco-energy smart cards", several devices were built, taking into account the effective area and the type of electrode used in the CCL. An extra test was done in order to study the electrostatic influence of the electrodes, when coupled, in the final output of the device. For that a device was built with two CCL coupled and encapsulated. The results shown in **Figure A.4.1** revealed that, compared to the devices with an AL, no substantial performance is verified.

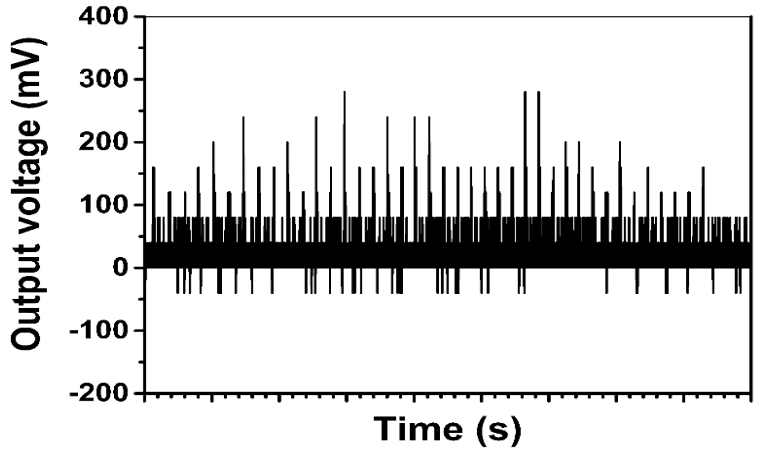

Figure A.4.1 - Output measurement taken on simple paper coupled with two electrodes showed no substantial performance compared to device based on functionalized paper

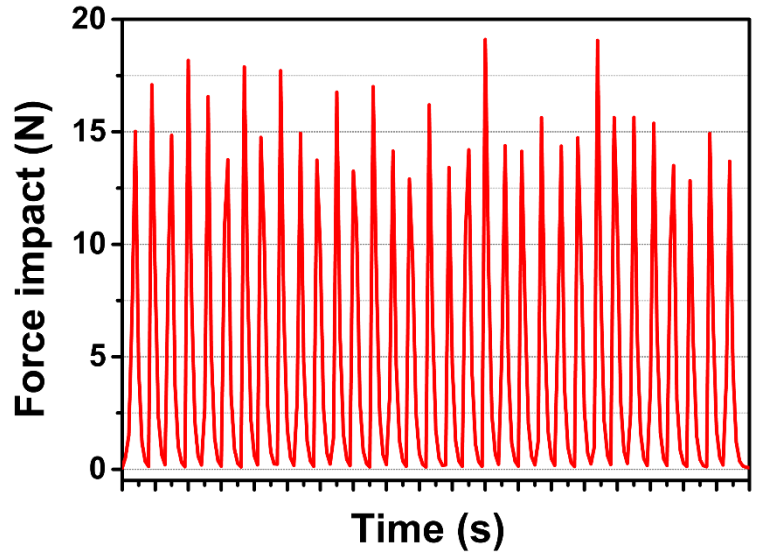

Figure A.4.2 - Test for average force impact that can be employed through hand patting in general. The measurement was done several times by an average male human hand (70 kg weight, 170 cm height).This measurement was made by making use of a tensile machine (Shimadzu AG-50kNG).

An Arduino board (Arduino Uno Rev3 (ATMega 328P)) was programmed with a force sensor (FSR 406 by Interlink Electronics) so that when force was applied onto the "eco-energy smart cards" the arduino software would write the magnitude of the force applied.

Arduino software code

The Arduino software code for force magnitude measurement is described below.

```
int fsrPin = 0;
int fsrReading;
int fsrVoltage;
unsigned long fsrResistance;
unsigned long fsrConductance;
long fsrForce;

#define fsrpin A0
#define led1 2
#define led2 3
#define led3 4
#define led4 5
#define led5 6
#define led6 7

void setup(void) {
  Serial.begin(9600);


  pinMode(led1, OUTPUT);
  pinMode(led2, OUTPUT);
  pinMode(led3, OUTPUT);
  pinMode(led4, OUTPUT);
  pinMode(led5, OUTPUT);
  pinMode(led6, OUTPUT);
  }

void loop(void)
```

```
{
   fsrReading = analogRead(fsrPin);

 if (fsrReading == 0) {
}
 else
 {

  fsrReading = analogRead(fsrpin);

  Serial.println(fsrReading);

  if (fsrReading > 200) {
    digitalWrite(led1, HIGH);
  }
  else digitalWrite(led1, LOW);
  if (fsrReading > 450) {
    digitalWrite(led2, HIGH);
  }
  else digitalWrite(led2, LOW);
  if (fsrReading > 550) {
    digitalWrite(led3, HIGH);
  }
  else digitalWrite(led3, LOW);
  if (fsrReading > 650) {
    digitalWrite(led4, HIGH);
  }
  else digitalWrite(led4, LOW);
  if (fsrReading > 800) {
    digitalWrite(led5, HIGH);
  }
```

```
  else digitalWrite(led5, LOW);
  if (fsrReading > 900) {
    digitalWrite(led6, HIGH);
  }
  else digitalWrite(led6, LOW);

  Serial.print("Analog reading = ");
  Serial.println(fsrReading);



  fsrVoltage = map(fsrReading, 0, 1023, 0, 5000);
  Serial.print("Voltage reading in mV = ");
  Serial.println(fsrVoltage);

  if (fsrVoltage == 0) {
    Serial.println("No pressure");
  }
 else {

    fsrResistance = 5000 - fsrVoltage;
    fsrResistance *= 10000;
    fsrResistance /= fsrVoltage;
    Serial.print("FSR resistance in ohms = ");
    Serial.println(fsrResistance);

    fsrConductance = 1000000;
    fsrConductance /= fsrResistance;
    Serial.print("Conductance in microMhos: ");
    Serial.println(fsrConductance);
```

```
   if (fsrConductance <= 1000) {
     fsrForce = fsrConductance / 80;
     Serial.print("Force in Newtons: ");
     Serial.println(fsrForce);
   } else {
     fsrForce = fsrConductance - 1000;
     fsrForce /= 30;
     Serial.print("Force in Newtons: ");
     Serial.println(fsrForce);
   }
 }
 Serial.println("--------------------");
}
}
```

Supporting Real-time video:

1. Supporting Video SV1: Real-time video of touch-interactive energy harvesting from self-powered "eco-energy smart card".

https://drive.google.com/file/d/1cL2_zkrdDHPvP3s2WEnZcLB31-XHmV7N/view?usp=sharing

2. Supporting Video SV2: Real-time video of instantaneous powering up 40 LEDs in series configuration by touch-interactive energy harvesting from self-powered "eco-energy smart card"

https://drive.google.com/file/d/1N86oWoPspyAqdPscTTnuRqFMB481tcDr/view?usp=sharing

3. Supporting Video SV3: Real-time video of LEDs, displaying FCT, in series configuration by touch-interactive energy harvesting from self-powered "eco-energy smart card"

https://drive.google.com/file/d/1Y1-f9KCnJCCzFmhFvmJ4RCt5O7_ysZqI/view?usp=sharing

4. Supporting Video SV4: Real-time video of commercial humidity sensor powering up after charging a 47 µF capacitor until 2V.

https://drive.google.com/file/d/1r9LRNtKAzyNWx_5NfMsdjfQZIdyfsWXi/view?usp=sharing

Annex 5. – “Eco-Energy Smart Card” Real-Field Applications

The electrical performance of the “eco-energy smart card” is dependent on four factors: effective area of AL, magnitude of the force applied, frequency of the force and the type of electrode used in the CCL. In order to study the current density and power density of the device, the following system was put into place. The system (**Figure A.5.1**) consisted in a signal rectifier in series with several resistances (values ranging from 55 kΩ and 150 MΩ) and an oscilloscope.

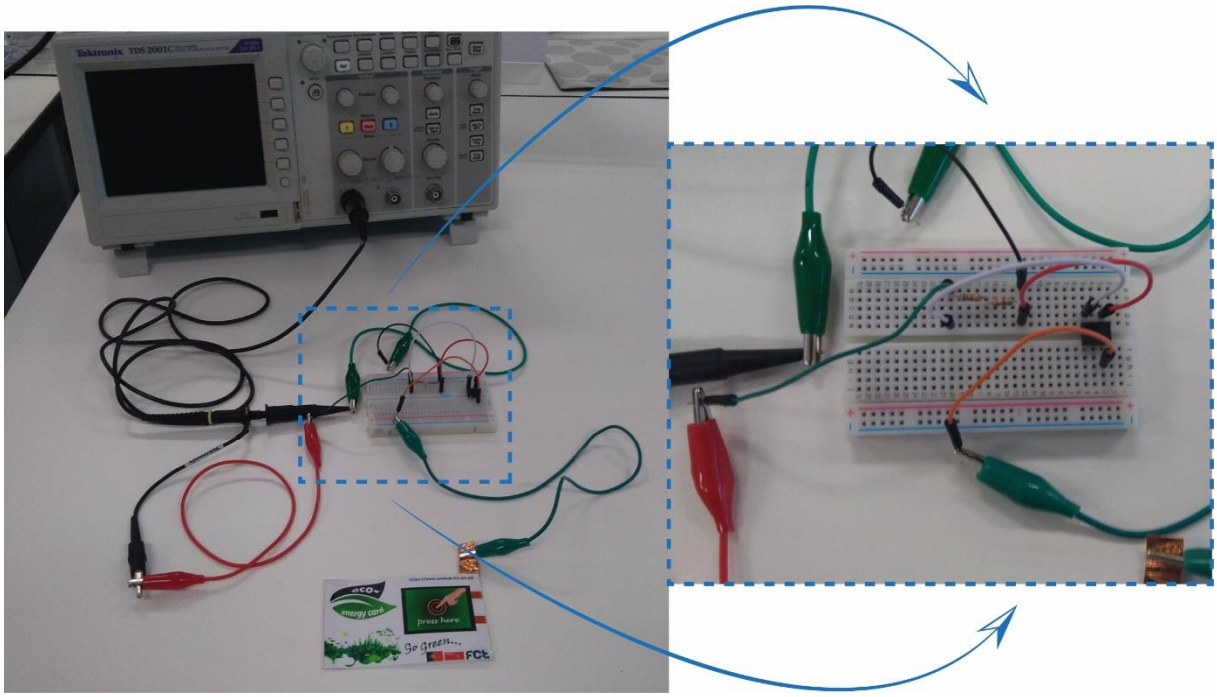

Figure A.5.1 - Snapshot of the rectifying circuit employed for determination of the current density and power density curves

Using the “eco-energy smart cards” a commercial humidity-sensor was powered up, as well as several blue LEDs, in many configurations, and five white LEDs (1.5 W), in series. (**Figure A.5.2**)

Figure A.5.2 - Instantaneous powering of 5 white LEDs (1.5W).